



**HAL**  
open science

## **On the generation and degradation of emerged coral reef terrace sequences: First cosmogenic $^{36}\text{Cl}$ analysis at Cape Laundi, Sumba Island (Indonesia)**

Denovan Chauveau, Christine Authemayou, Kevin Pedoja, Stéphane Molliex, Laurent Husson, Denis Scholz, Vincent Godard, Anne-Morwenn Pastier, Gino de Gelder, Sri Yudawati Cahyarini, et al.

### **► To cite this version:**

Denovan Chauveau, Christine Authemayou, Kevin Pedoja, Stéphane Molliex, Laurent Husson, et al.. On the generation and degradation of emerged coral reef terrace sequences: First cosmogenic  $^{36}\text{Cl}$  analysis at Cape Laundi, Sumba Island (Indonesia). *Quaternary Science Reviews*, 2021, 269, pp.107144. <10.1016/j.quascirev.2021.107144>. <hal-03350633>

**HAL Id: hal-03350633**

**<https://normandie-univ.hal.science/hal-03350633v1>**

Submitted on 16 Oct 2023

HAL is a multi-disciplinary open access archive for the deposit and dissemination of scientific research documents, whether they are published or not. The documents may come from teaching and research institutions in France or abroad, or from public or private research centers.

L'archive ouverte pluridisciplinaire HAL, est destinée au dépôt et à la diffusion de documents scientifiques de niveau recherche, publiés ou non, émanant des établissements d'enseignement et de recherche français ou étrangers, des laboratoires publics ou privés.



Distributed under a Creative Commons CC BY-NC 4.0 - Attribution - Non-commercial use - International License

1       **On the generation and degradation of emerged coral reef terrace sequences:**  
2               **first cosmogenic  $^{36}\text{Cl}$  analysis at Cape Laundi, Sumba Island (Indonesia)**

3  
4       Denovan Chauveau<sup>a</sup>, Christine Authemayou<sup>a</sup>, Kevin Pedoja<sup>b</sup>, Stéphane Molliex<sup>a</sup>, Laurent  
5       Husson<sup>c</sup>, Denis Scholz<sup>d</sup>, Vincent Godard<sup>e</sup>, Anne-Morwenn Pastier<sup>f</sup>, Gino de Gelder<sup>c</sup>, Sri  
6       Yudawati Cahyarini<sup>g</sup>, Mary Elliot<sup>h</sup>, Michael Weber<sup>d</sup>, Lucilla Benedetti<sup>e</sup>, Marion Jaud<sup>a</sup>, Audrey  
7       Boissier<sup>i</sup>, Vera Christanti Agusta<sup>g</sup>, Sonny Aribowo<sup>c</sup>, Ann. F. Budd<sup>i</sup>, Danny Hilman Natawidjaja<sup>g</sup>,  
8       A.S.T.E.R. Team<sup>e</sup>

9  
10       <sup>a</sup>LGO, IUEM, CNRS, UMR 6538, Université de Bretagne Occidentale, Plouzané, France

11       <sup>b</sup>M2C, UMR6143, UnivCaen-Normandie, Caen, France

12       <sup>c</sup>ISterre, CNRS, UMR 5275, Université de Grenoble Alpes, Grenoble, France

13       <sup>d</sup>Institut für Geowissenschaften, Johannes-Gutenberg-Universität Mainz, Mainz, Germany

14       <sup>e</sup>CEREGE, CNRS-IRD, UMR 34, Aix-Marseille Université, Aix-en-Provence, France

15       <sup>f</sup>GFZ German Research Centre for Geosciences, Earth Surface Process Modelling, Potsdam, Germany

16       <sup>g</sup>Research Center for Geotechnology, Indonesian Institute of Science, LIPI, Bandung, Indonesia

17       <sup>h</sup>LPG, CNRS, UMR 6112, Université de Nantes, Nantes, France

18       <sup>i</sup>IFREMER, Géosciences Marines, Centre de Brest, Plouzané, France

19       <sup>j</sup>Department of Earth and Environmental Sciences, University of Iowa, Iowa City, USA

20

21       **Keywords:** Quaternary; Coral reef terrace;  $^{36}\text{Cl}$  cosmogenic isotope; Denudation rate;  
22       U-Th series; Coastal erosion; MIS 5; Southeastern Asia.

23

24       **Abbreviations:** Coral Reef Terrace (CRT); Marine Isotope Stage (MIS); Electron Spin  
25       Resonance (ESR).

26

27       **Abstract**

28

29 The emerged coral reef terraces sequence at Cape Laundi, on the north coast of  
30 Sumba Island (Indonesia), with at least 18 successive strandlines, remains poorly  
31 dated in spite of numerous previous data. The age discrepancies within these coral  
32 reef terraces (CRTs) were previously explained by their polycyclic nature, triggered by  
33 marine erosion and reoccupation of old coral colonies by new ones. This study aims at  
34 highlighting these processes, as well as the continental denudation that participates in  
35 the partial stripping of the thin superficial coral reef layer overlying the pre-existing  
36 surface, exhuming older coral colonies. For this purpose, we use a combined analysis  
37 of  $^{36}\text{Cl}$  cosmogenic concentrations, new  $^{230}\text{Th}/\text{U}$  ages, and previous dating in order to  
38 quantify denudation rates affecting the sequence and to highlight the role of marine  
39 erosion in reworking the lowest CRT surface. Our results demonstrate that 1) the  
40 lowermost CRT is composite, i.e., formed by different reefal limestone units  
41 constructed and eroded during successive highstands of the last interglacial, 2)  
42 following the last deglaciation, this CRT has been subjected again to coastal erosion  
43 and reoccupation during the Mid Holocene highstand, 3) its distal edge is affected by  
44 the current marine erosion and shows denudation rates higher by one to two orders of  
45 magnitude (from  $279 \pm 0.4$  to  $581 \pm 0.4$  mm ka<sup>-1</sup>) than the continental denudation  
46 values of higher CRTs ( $14.7 \pm 8.3$  mm ka<sup>-1</sup> on average), 4) at the scale of a single CRT  
47 surface, variations in continental denudation rates are caused by epikarstification  
48 roughness, 5) the distal edges have the highest continental denudation rate due to  
49 diffusion and regressive erosion produced by the runoff occurring along the steep  
50 downward cliff.

51

## 52 **1. Introduction**

53

54 Sumba is an actively rising island in Indonesia where an emerged coral reef terraces  
55 sequence records the progressive emergence of the island. The sequence at Cape  
56 Laundi, on the north coast of the island, reaches ~470 m in elevation and includes at  
57 least 18 successive coral reef terraces (CRTs). This sequence has a well-preserved  
58 and potentially valuable record of Quaternary sea level, paleoclimate and tectonics, for  
59 which dating of the CRTs is crucial. The previous studies of this CRTs sequence  
60 (Pirazzoli et al., 1991; 1993; Bard et al., 1996) have identified significant temporal  
61 discrepancies within the CRTs, i.e., different ages of corals within the same CRT and  
62 similar ages of corals on several CRTs. Pirazzoli et al. (1991; 1993) and Bard et al.  
63 (1996) proposed that the CRTs have a polycyclic nature in order to explain age  
64 diachronism (Fig. 1). Pirazzoli et al., (1993) suggested that marine erosion can reshape  
65 the CRT surface and promote the bioconstruction of a new coral-colony on an older  
66 one during sea level highstands (Fig. 1A). Bard et al. (1996) indicated that a decrease  
67 in the rate of uplift to a low rate would in recurrent similar relative sea levels, causing  
68 several phases of reef development on a pre-existing surface (Fig. 1B). The role of  
69 marine erosion on the morphogenesis of CRTs has been discussed since a long time  
70 (e.g., Chappell, 1974; Hearty et al., 2008). Despite the persistence in recent  
71 publications of a simplistic definition of CRTs as constructive marine terraces; it is now  
72 clearly accepted in many syntheses that a CRT surface results from the combination  
73 of bioconstruction, erosion at sea level and accumulation of the eroded sediments  
74 (Pirazzoli, 2005; Cabioch, 2011; Murray-Wallace and Woodroffe, 2014; Pedoja et al.,  
75 2018; Pastier et al., 2019).

76

77 Apart from the role of marine erosion and bioconstruction reoccupation, what is the  
78 role of continental denudation in age diachronism on the same CRT? On polycyclic

79 CRT, continental denudation could partially strip the thin superficial layer of a young  
80 fossil coral reef and exhume older corals in several places (Fig. 1C). Since the  
81 stratigraphy of the CRTs on Sumba is not described and is difficult to observe in the  
82 canyons that incise them, and since the preservation of paleo-soils is unlikely in the  
83 polycyclic CRTs by their subsequent marine abrasion during a new transgression, we  
84 have chosen to combine the cosmogenic  $^{36}\text{Cl}$  method (e.g., Lal, 1988; 1991; Bierman,  
85 1994), new  $^{230}\text{Th}/\text{U}$  dating and previous dating to highlight the processes of marine  
86 erosion, reoccupation and continental denudation affecting the CRTs of Cape Laundi.  
87 The  $^{36}\text{Cl}$  method has already been carried out on CRTs in Barbados, resulting in  
88 quantification of the continental denudation rate (Lal et al., 2005).

89

90 In this study, we measured the cosmogenic  $^{36}\text{Cl}$  isotopes concentration of 34 *in situ*  
91 surface samples collected from the oldest CRT to the current reef shelf and took  
92 several samples on each CRT from the inner edge to the lower cliff in order to detect  
93 variation of continental denudation on them (Figs. 1C; 2). Moreover, we analyzed the  
94  $^{36}\text{Cl}$  concentration in a  $2.5 \pm 0.1$  m deep core of the lowermost CRT to attempt to (1)  
95 constrain its exposure time to cosmic rays (i.e., the age at which it emerged) if the  
96 concentration of  $^{36}\text{Cl}$  decreases exponentially at depth (e.g., Braucher et al., 2011), or  
97 (2) to detect several exposure phases (i.e., reoccupation stages) by  $^{36}\text{Cl}$  concentration  
98 peaks at depth (Figs. 1A; 1B). We conducted  $^{230}\text{Th}/\text{U}$  dating of two coral colonies in  
99 growth position collected on the Holocene landform and used these  $^{230}\text{Th}/\text{U}$  ages to  
100 calculate a coastal denudation rate from the  $^{36}\text{Cl}$  concentrations of samples taken from  
101 the top of the active Holocene sea cliff. We discuss our results in terms of 1) their  
102 comparison with global trends, as well as 2) continental denudation rates of carbonates

103 and their heterogeneity, and 3) the influence of marine erosion and constructive  
104 reoccupation components on CRT morphogenesis.

105

## 106 **2. Background**

### 107 **2.1. Emerged coral reef terrace sequences**

108

109 Morphologically, a CRT is an expanse of reefal limestone with a surface that is flat or  
110 slightly sloping seawards, limited by a change in slope seaward and landward.  
111 Seaward, the change in slope (i.e., a distal edge associated with a more or less steep  
112 cliff; Fig. 2), is usually described as the paleo reef crest (e.g., Pirazzoli et al., 1991;  
113 Rovere et al., 2016). Landward, at the inner edge, a CRT is characterized by a break  
114 in slope, sometimes interpreted as a shoreline angle suggesting the erosional sea cliff  
115 nature (e.g., Speed and Cheng, 2004; Pedoja et al., 2018). This break in slope provides  
116 a rather good marker for relative sea level, usually associated with the sea level  
117 highstands of former interglacial stages (e.g., Pirazzoli et al., 1993; Bard et al., 1996;  
118 Pedoja et al., 2018).

119

120 CRTs are geomorphologic plane surfaces encountered in the tropical zones and are a  
121 type of marine terraces in the broadest sense of the term (Schwartz, 2006; Murray-  
122 Wallace and Woodroffe, 2014; Pedoja et al., 2018). When the global sea level falls too  
123 rapidly and/or the reef is lifted by tectonic movements or glacial isostatic adjustment, it  
124 emerges, dies, and fossilizes, forming a CRT. The joint effects of sea level oscillations  
125 and tectonic uplift can result in the generation of a CRTs sequence with a staircase  
126 geometry (Fig. 2) (e.g., Chappell, 1974; Pirazzoli, 2005). Since the 19<sup>th</sup> century, such  
127 sequences have been described in the Caribbean province (Haiti, Cuba, Barbados;

128 e.g., Crosby, 1883; Simms, 2021; Thompson and Creveling, 2021), in the Indo-Pacific  
129 province (Indonesia, Papua New Guinea, Japan, Fiji, Philippine, and other islands or  
130 archipelagos; e.g., Darwin, 1842; Daly, 1915; Pirazzoli et al, 1993; Pedoja et al, 2018),  
131 as well as alongshore the Red Sea (Scholz et al., 2004; Murray-Wallace and  
132 Woodroffe, 2014; Pedoja et al., 2011; 2014; Obert et al., 2019).

133

134 The stratigraphy and morphology of a CRT, as well as these of a sequence, result from  
135 interactions between the vertical land motion, absolute and relative sea level  
136 variations, slope of the foundations, erosion processes (either mechanical or chemical  
137 and marine or continental in origin), reef bioconstruction, subsequent accumulation of  
138 eroded sediments and reef reoccupation (e.g., Pirazzoli, 2005; Cabioch, 2011; Husson  
139 et al., 2018; Pedoja et al., 2018; Pastier et al., 2019). Rates of reef growth, marine  
140 erosion and sedimentation may vary spatially due to a change in shoreline direction  
141 (e.g., from a bay to a cape), resulting in a modification in the final geometry of the  
142 sequence (Fig. 2). Thus, one CRT with a continuous high fossil sea cliff (>10 m; CRT  
143 I in figure 2) can include numerous secondary or intermediate CRTs (CRTs I<sub>1</sub> and I<sub>2</sub> in  
144 figure 2) with or without low (<10 m), eroded, fossil sea cliffs and various reefal  
145 limestone units (Fig. 2) (Hantoro et al., 1989; Pirazzoli et al., 1993; Speed and Cheng,  
146 2004). Geomorphologically, these compound CRTs are named main CRTs (e.g.,  
147 Pirazzoli et al., 1993). These main CRTs, sometimes morphologically forming a single  
148 CRT (CRT I in figure 2), may contain coral colonies sampled in growth position on their  
149 surface providing ages associated with different Marine Isotope Stage (MIS) (the  
150 different reefal limestone units on CRT I in figure 2) (e.g., Pirazzoli et al., 1993; Bard  
151 et al., 1996). When such a diachronism is observed, these CRTs are named composite  
152 CRTs (e.g., Kindler et al., 2007).

153

154

## **2.2. Sumba Island**

155

### **2.2.1. Tectonic and geologic setting**

156

157 Sumba is a 220 km-long and 65 km-wide island located in the lesser Sunda  
158 Archipelago, Indonesia. It is located near the transition from oceanic subduction in the  
159 West, along the Java trench, to the collision of the Banda arc with the continental  
160 Indian-Australian plate in the East (Fig. 3) (Hinschberger et al., 2005). The Cretaceous  
161 to Oligocene crystalline basement is almost entirely covered by Miocene and Pliocene  
162 deposits (Abdullah et al., 2000). The Miocene rocks consist of carbonate platform  
163 deposits to the west that evolve eastward into deep basin deposits (Von der Borch et  
164 al., 1983; Van der Werff et al., 1995). Since the late Miocene/Pliocene, the  
165 convergence between the Eurasian and Indian-Australian plates has been driving  
166 shortening and uplift in the fore-arc domain (e.g., Harris, 1991; Fortuin et al., 1997;  
167 Haig, 2012; Tate et al., 2014). In Sumba island, the Quaternary uplift is recorded by a  
168 ~350 km long CRTs sequence (e.g., Pirazzoli et al., 1991; Bard et al., 1996). The  
169 Sumba sequence is nearly continuous, interrupted only locally by large rivers. It spans  
170 approximately two-thirds of the island's shores, mostly along its northern coast and the  
171 eastern and western tips of the island (Hantoro, 1992; Fleury et al., 2009; Nexer et al.,  
172 2015; Authemayou et al., 2018).

173

174

### **2.2.2. Climate and hydrodynamics**

175

176 The climate affecting Sumba island is tropical, with humid winters and dry summers,  
177 albeit relatively dry compared to other parts of Indonesia (Prasetia et al., 2013). The

178 mean annual precipitation in Sumba is  $1077 \pm 406$  mm a<sup>-1</sup> (average over the 1998-  
179 2009 period of TRMM data; e.g., Kummerow et al., 2000).

180

181 The tides of Sumba Island have a range of ~3.5 m (Colas and Sutherland, 2001;  
182 Alfonso-Sosa, 2016; Hibbert et al., 2016). Nevertheless, our study site (Cape Laundi)  
183 is located on the northern, leeward side of the island which is only exposed to short  
184 wavelength fetch swell (<10 s, i.e., windswell) (Butt et al., 2004).

185

### 186 **2.2.3. Previous studies on the Cape Laundi emerged coral reef** 187 **terraces sequence**

188

189 Cape Laundi was first mapped by Jouannic et al., (1988). It reaches ~470 m in  
190 elevation and has a staircase shape with six main CRTs separated by continuous high  
191 (>10 m) fossil sea cliffs (Pirazzoli et al., 1993). Each main CRT includes several  
192 intermediate CRTs (Hantoro et al., 1989; Pirazzoli et al., 1993). Marine erosion was  
193 detected by Pirazzoli et al. (1991; 1993) from the presence of marine notches in the  
194 inner edges of main CRTs, and the observation of coral development surfaces marked  
195 by traces of subsequent erosion observed along several canyons transversely cutting  
196 the slope of the sequence.

197

198 Approximately fifty coral colonies have been dated (using U/Th and ESR dating  
199 methods) on the surface of the five lowest main CRTs (T<sub>I</sub> to T<sub>IV1</sub> in Pirazzoli et al.,  
200 1993). These ages were correlated to eustatic peaks of the highstands associated,  
201 respectively from the oldest to the youngest, to MIS 15 ( $610 \pm 10$  ka), MIS 11 ( $390 \pm$   
202  $30$  ka), MIS 9 ( $325 \pm 18.5$  ka), MIS 7 ( $239.5 \pm 8.5$  ka), MIS 5 ( $122 \pm 6$  ka) and MIS 1

203 (mid Holocene highstand,  $6 \pm 2$  ka) (Pirazzoli et al., 1993; Bard et al., 1996). The oldest  
204 dated CRT, named  $T_{IV1}$  in previous studies, yielded ESR ages of  $584 \pm 88$  ka and  $603$   
205  $\pm 90$  ka and was corresponding to MIS 15 (Pirazzoli et al., 1991; 1993). At higher  
206 elevations than  $T_{IV1}$ , the ages of the successive CRTs were extrapolated assuming a  
207 constant uplift rate (i.e.,  $0.49 \pm 0.01$  mm a<sup>-1</sup>; Pirazzoli et al., 1993). The upper, undated  
208 CRTs were thus correlated to sea level highstands up to ~1 Ma, i.e., MIS 29 (Jouannic  
209 et al., 1988; Pirazzoli et al., 1991; 1993; Hantoro, 1992; Bard et al., 1996).

210

211 However, a number of temporal discrepancies emerged with the dating done by  
212 Pirazzoli et al. (1991; 1993). Firstly, U-series ages of corals from the same CRT are  
213 diachronic (e.g., ages of ~82 ka and ~138 ka from CRT  $I_1$ ). Secondly, the same U-  
214 series ages came from corals on at least three CRTs (e.g., MIS 5e ages on CRTs  $I_1$ ,  
215  $I_2$ , and  $II_2$ ), and thirdly, U-series ages and ESR ages of corals from the same CRT do  
216 not always match with one another. Thereafter, TIMS U-series dating of corals (Bard  
217 et al., 1996) specified the diachronism (i.e., MIS 5a, 5c, and 5e ages on CRT  $I_1$ ; MIS  
218 5c, 5e and pre-MIS 5e ages on CRT  $I_2$ ).

219

220 Bard et al. (1996) interpreted the age inconsistencies to reflect the decrease in uplift  
221 rates during a significant period of the late Pleistocene. Very low uplift rates induce  
222 negligible uplift of the lowest CRTs before the next transgression, resulting in one or  
223 more reoccupation events in which new coral can grow on the pre-existing CRT (Fig.  
224 1B). Combining <sup>230</sup>Th/U dating with numerical modeling, Bard et al. (1996) estimated  
225 an uplift rate ranging from 0.2 to 0.5 mm a<sup>-1</sup> and proposed also a polycyclic nature for  
226 several CRTs (up to MIS 7). Low uplift rates (0.2 mm a<sup>-1</sup>) allow coral colonies of a CRT  
227 to be recovered by younger ones during a new transgression. But, to obtain the 0.2

228 mm a<sup>-1</sup> minimum uplift rate, the previous authors correlated the inner edge of the  
229 lowermost main CRT ( $23 \pm 2$  m) to MIS 5e, taking into account only the oldest <sup>230</sup>Th/U  
230 ages. This hypothesis implies that during the MIS 5c and 5a highstands, coastal  
231 erosion has been negligible to preserve the morphology of the MIS 5e CRT.

232

233 Pirazzoli et al. (1993) interpreted the age inconsistencies to reflect marine erosion.  
234 Indeed, they suggested that eustatic sea level fluctuations with efficient marine  
235 abrasion superimposed on a regular uplift trend of 0.5 mm a<sup>-1</sup> must have led sea level  
236 to reach nearly the same position several times and the development of  
237 bioconstructions differing in age as much as 100 ka on the same CRT (Fig. 1A). The  
238 present altitude of dated CRTs allowed Pirazzoli et al. (1991; 1993) to propose an uplift  
239 rate trend of  $0.49 \pm 0.01$  mm a<sup>-1</sup>.

240

### 241 **3. Methods**

#### 242 **3.1. Mapping, bathymetry, and sampling**

##### 243 **3.1.1. Onshore and offshore data**

244

245 We mapped the inner edges of the CRTs at Cape Laundi using a high resolution (2 m)  
246 Digital Elevation Model (DEM) produced from stereoscopic satellite images (Pleides,  
247 CNES) with MicMac freeware (e.g., Rupnik et al., 2016). We acquired topographic and  
248 bathymetric profiles, using a real kinematic differential global positioning system (RTK  
249 DGPS) onshore, and a Humminbird 700 series sonar offshore (Fig. 4). Onshore, our  
250 profiles were carried out perpendicular to the main inner edges of the successive  
251 CRTs, parallel to those proposed by Pirazzoli et al. (1993) and starting from the mean

252 sea level. Profile 1 crosses the whole CRTs sequence and Profile 2 focuses on the  
253 lowest CRTs (Fig. 4).

254

255 The roughness of the successive CRTs increases with elevation and therefore age  
256 because of continental denudation (e.g., epikarst). This roughness is the main source  
257 of error in elevation, far beyond instrumental errors. Consequently, we assigned an  
258 elevation uncertainty to all the field measurements as a function of the amplitude of the  
259 observed natural landform roughness;  $\pm 0.5$  m for low standing landforms ( $<250.5 \pm$   
260  $0.5$  m in elevation);  $\pm 1.5$  m on the summit of Cape Laundi and the upper CRTs ( $>250.5$   
261  $\pm 0.5$  m in elevation) (Fig. 5).

262

### 263 **3.1.2. Sampling strategy**

264

265 We extracted samples for  $^{230}\text{Th}/\text{U}$  dating, by drilling two coral colonies in growth  
266 positions (samples SUM17-10 and SUM17-13) located on the Holocene CRT (H), near  
267 the modern shore (Figs. 3; 4). From the base (CRT H) to the summit of Cape Laundi  
268 (CRT VI), we collected 34 samples from the non-vegetated surfaces of the reefal  
269 limestones forming the CRTs for cosmogenic  $^{36}\text{Cl}$  analysis (Figs. 3; 4). To investigate  
270 the potential variability of denudation rates across a given CRT, we collected samples,  
271 when possible, from 1) the inner edge, 2) the main surface and 3) the distal edge (Fig.  
272 2).

273

274 Below  $167.6 \pm 0.5$  m, intermediate CRTs are distinguishable in the field through fossil  
275 sea cliffs ( $\sim 3$  m in height), separated by narrow (80-430 m wide) flat surfaces (Fig. 6).  
276 For such CRTs, the distances between two successive sampling sites (i.e., inner edge,

277 main surface, and distal edge) typically range from 20 to 100 m. The CRTs higher than  
278  $167.6 \pm 0.5$  m are wider, typically from  $\sim 330$  to  $\sim 1\ 300$  m wide, and our sampling  
279 interval is  $\sim 500$  m.

280

281 To constrain exposure age (i.e., the age at which the CRT emerged), in the case that  
282 the concentration of  $^{36}\text{Cl}$  decreases exponentially at depth (e.g., Braucher et al., 2011)  
283 or to highlight several exposure events (i.e., reoccupation stages), in the case that  $^{36}\text{Cl}$   
284 concentration peaks at a certain depth, we drilled the lowermost CRT ( $I_1$ ) to get a  
285 continuous  $\sim 2.5$  m deep borehole (Fig. 4) (e.g., Braucher et al. 2009; 2011; Hein et al.  
286 2009; Schaller et al. 2009). Because of the heterogeneity and porosity of the fossil  
287 reefal limestone, our borehole broke into pieces, preventing us from precisely knowing  
288 the depths of most of the individual samples. Only the depth of the deepest material  
289 recovered from  $2.5 \pm 0.1$  m below the surface of the CRT and the surface sample were  
290 considered.

291

### 292 **3.2. Cosmogenic nuclides**

293

294 The  $^{36}\text{Cl}$  cosmogenic concentration in rocks ( $N(z,t)$ ,  $\text{g}^{-1}$  atom) as a function of depth ( $z$ ,  
295 cm) and time ( $t$ , year) can be expressed as follows (Stone et al., 1994):

296

$$297 \quad \frac{\partial N(z,t)}{\partial t} = P(z) - \lambda N(z,t) - \varepsilon \frac{\partial N(z,t)}{\partial z} \quad (1)$$

298

299  $z$  is the depth of a sample. Here, all but one sample (from the bottom of the core in the  
300 lowermost CRT) have been collected from exposed bedrock surfaces ( $z=0$ ), under a  
301 surface that denudes at a rate  $\varepsilon$  ( $\text{cm a}^{-1}$ ).  $P(z)$  is the total production rate of  $^{36}\text{Cl}$  (atom

302  $\text{g}^{-1} \text{rock a}^{-1}$ ), depending on 1) the cosmic radiation (itself affected by the following  
303 parameters: latitude, elevation, topographic shielding, self-shielding (i.e., sample  
304 thickness and depth)) passing through a rock of thickness  $z$  and 2) on the composition  
305 of the rock (Gosse and Phillips, 2001).  $\lambda$  is the decay constant of  $^{36}\text{Cl}$  ( $\lambda = 2.303 \cdot 10^{-6}$   
306  $\text{a}^{-1}$ ).

307

308 For all 34 samples, we selected the carbonate matrix containing as few coral fragments  
309 as possible. Density measurements on these matrix samples averaged  $2.5 \text{ g cm}^{-3}$ .  
310 Each sample was washed and the fraction 250-1000  $\mu\text{m}$  extracted. About  $\sim 100 \text{ g}$  of  
311 each sample was then used for chemical analysis. We used a standard chlorine  
312 extraction protocol, which includes several steps of leaching, designed to remove labile  
313 Cl of meteoric origin from mineral surfaces (Stone et al., 1996; Merchel et al., 2008;  
314 Schlagenhauf et al., 2010). More precisely, the procedure involved a cleaning process  
315 by ultrapure water to remove any suspended particles, followed by a partial dissolution  
316 process in 2M  $\text{HNO}_3$ . Samples were then spiked with  $\sim 270 \mu\text{g}$  of an enriched  $^{35}\text{Cl}/^{37}\text{Cl}$   
317 solution in order to determine the  $^{35}\text{Cl}$  natural content. Then, the sample was fully  
318 dissolved in 2M  $\text{HNO}_3$ . Residues were filtered from the solution and weighted. 1 ml  
319 solution aliquot was collected from the filtered solution for Ca determination. Then, Cl  
320 was precipitated as AgCl using  $\text{AgNO}_3$ . The precipitate was dissolved with ammonia  
321 and sulfur was reduced by the addition of a saturated  $\text{Ba}(\text{NO}_3)_2$  solution. Afterwards,  
322 the solution was filtered and a second precipitation of AgCl was performed with  $\text{HNO}_3$ .  
323 The dried AgCl was finally measured with Accelerator Mass Spectrometry (AMS) at  
324 CEREGE (Centre de Recherche et d'Enseignement de Géosciences de  
325 l'Environnement) in Aix-en-Provence (France).  $^{36}\text{Cl}$  production and denudation rates  
326 were calculated following Schimmelpfennig et al. (2009) taking into account Sea-Level-

327 High-Latitude production rates for rapid neutron spallation reactions ( $42.2 \pm 2$  atoms  
328  $^{36}\text{Cl}$  ( $\text{g Ca}^{-1} \text{ a}^{-1}$ ); Braucher et al., 2011; Schimmelpfennig et al., 2011; 2014), negative  
329 muons (Heisinger et al., 2002), the rate of epithermal neutron production from fast  
330 neutrons (Phillips et al., 2001) and the production from radiogenic neutrons (Fabryka-  
331 Martin, 1988; Phillips and Plummer, 1996) (more information related to  $^{36}\text{Cl}$  production  
332 is detailed in Appendix "A" of Schimmelpfennig et al., 2009). Topographic shielding  
333 was calculated for each sample using the topographic shielding add-in for ArcGIS  
334 software (Codilean, 2006). The scaling factors are calculated with CosmoCalc 1.7  
335 macro (Vermeesch, 2007; Dunai, 2010). Major oxides ( $\text{SiO}_2$ ,  $\text{TiO}_2$ ,  $\text{Al}_2\text{O}_3$ ,  $\text{Fe}_2\text{O}_3$ ,  $\text{MnO}$ ,  
336  $\text{MgO}$ ,  $\text{CaO}$ ,  $\text{Na}_2\text{O}$ ,  $\text{K}_2\text{O}$ ,  $\text{P}_2\text{O}_5$ ) and trace elements (Li, Be, Mo, Ba, Sm, Gd, Pb, Th, U,  
337 B, Sc, Cr, Cr, Co, Ni, Rb, Sr) have been measured on the bulk samples (i.e., the size  
338 fraction  $< 250 \mu\text{m}$  collected after crushing), respectively by an ICP AES-Ultima 2-Jobin  
339 Yvon and an HR-ICP-MS Element XR, at the LGO (Laboratoire Géosciences Océan,  
340 IUEM) in Brest (France) to determine their impact on the  $^{36}\text{Cl}$  production rate. The  $\text{CO}_2$   
341 concentration in samples is determined by weighing the samples, dissolving them in a  
342 Gas bench and measuring the  $\text{CO}_2$  produced (Pôle de Spectrométrie Océan,  
343 Plateforme Isotopes Stables, IUEM, Brest, France).

344

345 The interaction of secondary cosmic rays with rocks exposed in the Earth's surface  
346 produces cosmogenic isotopes (Gosse and Phillips, 2001). Four major interactions are  
347 responsible for the production of cosmogenic isotopes, in order of importance:  
348 spallation, muon capture, neutron activation, and alpha particle interaction (Bierman,  
349 1994). Except for the production of  $^{36}\text{Cl}$  by neutron capture, which peaks at a shallow  
350 depth rather than at the surface, cosmogenic isotope production rates decrease  
351 exponentially with depth until they stabilize (Stone et al., 1998). The abundance of

352 cosmogenic isotopes increases with exposure time until steady state, when production  
353 and decay of the cosmogenic isotope are balanced (Schlagenhauf et al., 2010). More  
354 precisely, when bedrock surfaces are exposed to cosmic ray particles and denuded at  
355 a constant rate for long enough, the induced cosmogenic nuclide production  
356 equilibrates the losses due to radioactive decay and mass removal linked to  
357 denudation processes (Lal, 1991). The cosmogenic nuclide concentration reached at  
358 this steady state is inversely proportional to the denudation rate of the surface (e.g.,  
359 Granger and Riebe, 2014). The time it takes for the concentration of a cosmogenic  
360 nuclide to reach steady state depends mainly on the denudation rate. When this steady  
361 state is reached, it is possible to quantify the denudation rates without knowing the age  
362 of the surface because for any age taken, and for a given  $^{36}\text{Cl}$  concentration, the  
363 denudation rate will not vary anymore (e.g., Lal et al., 1991; Dunai, 2010). Conversely,  
364 for a surface sample that has not reached steady state and was taken on a surface  
365 without age constraint, there is an infinite number of age-denudation pair hypotheses  
366 that can explain the measured concentration. The denudation rate can be calculated  
367 by assuming or independently constraining an exposure age (e.g., using absolute  
368 chronological constraints such as  $^{230}\text{Th}/\text{U}$  ages) and vice versa. Also, constraining both  
369 exposure ages and denudation rates when steady state is not reached is possible by  
370 fitting a theoretical depth profile, calculated from measured surface and depth  
371 concentrations (Braucher et al. 2009; 2011; Hein et al. 2009; Schaller et al. 2009).

372

373 In this study, the denudation rates were calculated from  $^{36}\text{Cl}$  concentrations assuming  
374 a range of absolute ages for CRTs proposed by Pirazzoli et al. (1991; 1993). We show  
375 that cosmogenic steady state has been reached for older CRTs than CRT II7  
376 (corresponding to ~137 m altitude; Fig. 6) because denudation rates remain

377 unchanged regardless of the chosen age for the CRT. Thus, the age hypotheses are  
378 useless to quantify denudation rates for these older CRTs (Section 4.4.). Samples on  
379 CRTs surfaces yield continental denudation rates (Fig. 1C), while samples from CRT  
380 H yield the quantification of marine erosion (Fig. 1A). Denudation rates are averaged  
381 over the time period necessary to erode to a depth equivalent to the neutron  
382 characteristic attenuation length (approximately 60 cm in a substrate with a density of  
383  $2.5 \text{ g cm}^{-3}$ ) (Von Blanckenburg, 2005).

384

### 385 **3.3. $^{230}\text{Th}/\text{U}$ dating**

386

387 On CRT H (Holocene), at the same sites as the lowest  $^{36}\text{Cl}$  samples (SUM18-46 and  
388 SUM18-47), we also sampled coral colonies of *Platygyra* (sample SUM17-10) and  
389 *Favites* (sample SUM17-13 drilled in a fossil tidal pool) in growth position for  $^{230}\text{Th}/\text{U}$   
390 dating (Fig. 4). These  $^{230}\text{Th}/\text{U}$  dating were done on CRT H in order to complete the  
391 bibliographic data and to be as close as possible to the cosmogenic nuclide samples  
392 to better discuss marine erosion processes. The two samples were mechanically  
393 cleaned with a micro-drill and then crushed. Coral samples were rinsed in MilliQ water  
394 and leached in 0.1 N bi-distilled HCL for 15-20 minutes in an ultrasonic bath. The  
395 cleaned samples were then crushed into powder and analyzed using a XRD Brucker  
396 D8 at the LCG (Laboratoire d'étude des "Cycles Géochimiques et Ressources",  
397 IFREMER) in Brest (France) to quantify the relative quantities of calcite and aragonite.  
398 We proceeded with  $^{230}\text{Th}/\text{U}$  dating only with two samples, consisting purely of  
399 aragonite (>99%).

400

401 Subsequently, the powders were dissolved in 7N HNO<sub>3</sub> and a mixed <sup>229</sup>Th-<sup>233</sup>U-<sup>236</sup>U  
402 spike was added to the solution and allowed to equilibrate. A detailed description of  
403 the calibration of the spike is given by Gibert et al. (2016). After drying down the  
404 solutions, the residues were treated with a mixture of concentrated HNO<sub>3</sub>, HCl, and  
405 H<sub>2</sub>O<sub>2</sub> to remove potential organic components. Then, the solutions were dried again  
406 and dissolved in 6N HCl. The fractions of U and Th were then separated from the  
407 CaCO<sub>3</sub> matrix as described by Yang et al. (2015). For mass spectrometric analysis,  
408 the U and Th fractions were dissolved in 2 ml of 0.8N HNO<sub>3</sub>. U and Th isotope analysis  
409 was performed by multi-collector inductively coupled plasma mass spectrometry at the  
410 Institute for Geosciences of the Johannes Gutenberg-University, Mainz (Germany),  
411 using a Thermo Fisher Scientific Neptune Plus MC-ICP-MS. A detailed description of  
412 the analytical procedures is given by Obert et al. (2016).

413

## 414 **4. Results**

### 415 **4.1. Cape Laundi: offshore and onshore landforms**

416

417 Improved DEM resolution, new bathymetric data and field observations allowed us to  
418 improve the mapping of Cape Laundi. The precise description of the coastal  
419 morphology is essential to better understand the processes of its formation and  
420 destruction. Offshore, two submerged ~200 m wide surfaces (named -l<sub>1</sub> and -l<sub>2</sub>; Fig. 6),  
421 were newly identified. Their morphology is consistent with paleo-lagoons: flat in their  
422 central part (at  $-38 \pm 1$  and  $-53 \pm 1$  m for -l<sub>1</sub> and -l<sub>2</sub>, respectively; Fig. 6) and convex at  
423 their distal part associated with submerged barrier reefs (at  $-31 \pm 1$  and  $-44 \pm 1$  m for -  
424 l<sub>1</sub> and -l<sub>2</sub>, respectively; Fig. 6). We interpret these bathymetric features as submerged  
425 CRTs.

426

427 Onshore, seven main CRTs were identified up to  $469.8 \pm 1.5$  m with six major fossil  
428 sea cliffs (Figs. 4; 5A; 6). Most of these main CRTs include intermediate CRTs. For  
429 example, CRT II, with an inner edge raised at  $136.8 \pm 0.5$  m, is composed of seven  
430 intermediate CRTs (II<sub>1</sub>, II<sub>2</sub>, II<sub>3</sub>, II<sub>4</sub>, II<sub>5</sub>, II<sub>6</sub>, II<sub>7</sub>) separated by low fossil sea cliffs (<10 m  
431 each). The lowermost main CRT (CRT I) is 550 m wide, has an inner edge raised at  
432  $23.2 \pm 0.5$  m, and includes of two intermediate CRTs (I<sub>1</sub>, I<sub>2</sub>) separated at  $6.4 \pm 0.5$  m  
433 by a ~3 m high fossil sea cliff. On profile 2, CRT I is only 200 m wide, its surface is  
434 irregular, and the two intermediate CRTs (I<sub>1</sub>, I<sub>2</sub>) are separated at  $7.6 \pm 0.5$  m by a ~15  
435 m high fossil sea cliff.

436

437 CRT I<sub>1</sub> consists of well-preserved smooth flat surfaces (Figs. 5C; 5D). In places, its  
438 surface is covered by centimeter-scale remnants of a sandstone layer including coral  
439 rubbles (Fig. 5E). The surface of CRT I<sub>2</sub> is irregular and exhibits some isolated smooth  
440 multi-centimetric carbonate surfaces attesting for the relatively quick formation of rough  
441 surfaces on the CRT. This superficial layer becomes rougher and thicker from CRT II<sub>2</sub>,  
442 where it reaches ~20 cm (Fig. 5B). At the highest CRTs, epikarstic roughness reaches  
443 1 to 2 m (Figs. 5F; 5G). Moreover, the roughness varies across the CRTs, between  
444 ~0.1 to ~2 m, i.e., the inner edges and the main surfaces of the CRTs are rather smooth  
445 whereas their distal edges are rougher (Fig. 5G).

446

447 Alongshore, Holocene landforms are represented by a conglomerate, remnants of  
448 limestone banks of fossil reef, and coral colonies in growth position, reaching  
449 approximately  $2 \pm 0.5$  m above mean sea level (Fig. 5C). Remnants of CRT H have a  
450 restricted width (~5 m) and are delimited seaward by active sea cliffs (Fig. 5C). On the

451 flat surface of CRT H, some fossil corals appear very well-preserved and most  
452 frequently located in circular depressions with their associated ramparts filled by a  
453 white and fresh carbonated matrix (Fig. 5I). The diameter of such circular landforms is  
454 generally ~1 m and we interpret them as fossil tidal pools (Fig. 5I) (Hoeksema, 2012).  
455 Fossil coral colonies samples within this Holocene emergent reef have been previously  
456 cross-dated from  $2.03 \pm 0.18$  to  $6.32 \pm 0.14$  (Jouannic et al., 1988; Pirazzoli et al.,  
457 1991, 1993; Bard et al., 1996). The modern reef flat (called  $I_0$  on Fig. 5B) is typical of  
458 a fringing reef, as previously interpreted by Bard et al. (1996). There are living corals  
459 on the reef crest (seaward), whereas landwards the reefal flat is covered by coral  
460 rubbles (Fig. 5J) and associated with beaches and/or mangroves at some sites.

461

#### 462 **4.2. $^{230}\text{Th}/\text{U}$ dating of the Holocene CRT**

463

464 The two fossil coral samples display  $^{238}\text{U}$  concentrations between 2.4 and 3 ppm (Table  
465 1). Low  $^{232}\text{Th}$  contents together with high ( $^{230}\text{Th}/^{232}\text{Th}$ ) activity ratios argue for a lack of  
466 significant detrital contamination. Both samples display initial  $\delta^{234}\text{U}$  values that agree  
467 within errors with a mean modern ocean water value of  $\delta^{234}\text{U} = 146.8 \pm 0.1\text{‰}$   
468 (Andersen et al., 2010), indicating closed system evolution and no evidence for  
469 diagenetic alteration. These coral colonies samples yielded  $^{230}\text{Th}/\text{U}$  ages of  $5.45 \pm 0.02$   
470 ka (sample SUM17-10) and  $2.13 \pm 0.01$  ka (sample SUM17-13) (Table 1).

471

#### 472 **4.3. Distribution of $^{36}\text{Cl}$ concentration at the scale of the emerged coral** 473 **reef terraces sequence**

474

475 The  $^{36}\text{Cl}$  concentrations obtained from the samples along profiles 1 and 2 range from  
476  $3.68 \pm 0.08$  to  $20.00 \pm 0.37 \cdot 10^5$  atoms  $\text{g}^{-1}$  rock and average at  $7.74 \pm 3.67 \cdot 10^5$  atoms  
477  $\text{g}^{-1}$  rock ( $n = 28$ ; Table 2). Given the overall uniform lithology and precipitation rate, the  
478 variability across the profile is higher than expected if all measured  $^{36}\text{Cl}$  concentrations  
479 have been controlled by steady erosion. The six measured  $^{36}\text{Cl}$  concentrations of  
480 samples from CRT I have low variability (with an average at  $5.54 \pm 0.67 \cdot 10^5$  atoms  $\text{g}^{-1}$   
481 rock) compared to the  $^{36}\text{Cl}$  concentration of all other/older samples (with an average  
482 at  $8.25 \pm 3.90 \cdot 10^5$  atoms  $\text{g}^{-1}$  rock). The  $^{36}\text{Cl}$  concentration measured at the base  
483 (sample SUM18-47:  $0.30 \pm 0.05 \cdot 10^5$  atoms  $\text{g}^{-1}$  rock) and on the top of the modern sea  
484 cliff (sample SUM18-46:  $0.38 \pm 0.08 \cdot 10^5$  atoms  $\text{g}^{-1}$  rock) are an order of magnitude  
485 lower than those measured on Pleistocene CRTs (I-VII) (Table 2). At the borehole site  
486 (Fig. 4), the  $^{36}\text{Cl}$  concentrations measured at the surface ( $C_{\text{surface}}$ ) and at a depth of  
487  $2.5 \pm 0.1$  m ( $C_{\text{2.5m}}$ ) are  $6.23 \pm 0.28$  and  $2.46 \pm 0.12 \cdot 10^5$  atoms  $\text{g}^{-1}$  rock, respectively  
488 (Table 2).

489

#### 490 **4.4. Denudation rates**

491

492 The time scales over which denudation rates are integrated (Von Blanckenburg, 2005)  
493 range from  $16.2 \pm 0.3$  (highest rate) to  $237.3 \pm 27.0$  ka (lowest rate) with an average  
494 of  $61.7 \pm 49.6$  ka ( $n = 66$ ). Denudation rates for the various CRTs of the sequence  
495 range from  $2.5 \pm 0.1$  to  $37.1 \pm 0.9$   $\text{mm ka}^{-1}$  (average at  $14.7 \pm 8.3$   $\text{mm ka}^{-1}$ ,  $n = 66$ )  
496 (Table 3; Fig. 6). Despite the different age hypotheses for CRT I, the denudation rates  
497 calculated are more uniform than those determined for the upper CRTs (Table 3; Fig.  
498 6). Denudation rates from the CRTs II<sub>2</sub>, II<sub>3</sub>, and II<sub>4</sub> are rather similar, irrespective of  
499 different age hypotheses (Table 3; Fig. 6). The results suggest that cosmogenic steady

500 state has been reached for older CRTs than II<sub>7</sub>; i.e., whatever the assigned age to the  
501 CRT, the calculated denudation rates for these CRTs do not vary much (Table 3; Fig.  
502 6).

503

504 The average denudation rates affecting the inner edges, main surfaces and distal  
505 edges of the CRTs are  $11.1 \pm 7.0$  (n = 16),  $14.3 \pm 6.8$  (n = 38), and  $20.8 \pm 8.6$  mm ka<sup>-1</sup>  
506 (n = 12) respectively. Denudation rates for CRTs main surfaces are widely dispersed  
507 and range from  $2.5 \pm 0.3$  (sample SUM18-37) to  $29.4 \pm 1.4$  mm ka<sup>-1</sup> (sample SUM16-  
508 8). Apart from the denudation rate calculated for sample SUM18-15 (Table 3),  
509 denudation rates affecting the inner edges of CRTs I<sub>1</sub>, II<sub>1</sub>, II<sub>4</sub>, II<sub>6</sub>, V, VI are similar to  
510 those of the fossil reef flats. Denudation rates for the distal edge of the CRTs are higher  
511 than rates from other parts of the landform. Since the number of denudation rate values  
512 is low, a non-parametric statistical test was performed (Kruskal-Wallis test) to  
513 determine whether denudation rates vary significantly by morphological location of the  
514 samples analyzed. The average rank of the calculated denudation rates is not  
515 statistically significantly different according to the morphological location of the  
516 samples ( $P_{\text{value}} = 0.26$ ). Thus, the morphology of the CRTs does not fully explain the  
517 heterogeneity of the calculated denudation rates.

518

519 Sample SUM18-46 was collected from the same surface (CRT H) of the samples used  
520 for <sup>230</sup>Th/U dating (SUM17-10 and SUM17-13) (Figs. 4; 5C). Considering <sup>230</sup>Th/U ages  
521 as the exposure time of the surface, we calculated denudation rates of  $279.0 \pm 0.4$  mm  
522 ka<sup>-1</sup> and  $581.0 \pm 0.4$  mm ka<sup>-1</sup> (Table 3). These denudation rates (average of  $430 \pm 214$   
523 mm ka<sup>-1</sup>; Table 3) near the sea level are much higher, by one to two orders of  
524 magnitude, than the denudation rates calculated for the other CRTs (I-VI).

525

## 526 **5. Discussion**

527

528 Significant denudation rates obtained at the sea level and on the CRTs sequence point  
529 to marine erosion and continental denudation as the cause of the age diachronism on  
530 a single CRT (Figs. 1A; 1B). This hypothesis also requires reef reoccupation over  
531 several highstands (R2 over R1 on figure 1). Our results provide the opportunity to  
532 discuss the dynamics of these processes at Cape Laundi. We first highlight the role of  
533 reef reoccupation processes and marine erosion in shaping CRTs. Then, we discuss  
534 continental denudation by comparing our data with denudation rates published for the  
535 Barbados and Puerto Rico CRTs (Lal et al., 2005), as well as for other carbonate  
536 landscapes (e.g., Spencer, 1985; Vasconcelos and Stone, 2000), and focusing on the  
537 variability of denudation rates.

538

### 539 **5.1. The genesis of the lowermost main CRT (I)**

#### 540 **5.1.1. Reefal limestone units overlapping**

541

542 Whatever the hypothesis to explain diachronous ages on the same CRT surface, the  
543 CRT internal architecture must be associated with a phenomenon of reef reoccupation  
544 over several highstands in order to have recent thin reef units stacked on older units  
545 (R2 over R1 in figure 1). In the borehole site of CRT 1, theoretically, if both measured  
546 samples belong to the same reefal limestone unit, the  $^{36}\text{Cl}$  concentration profile in  
547 depth (constrained by an erosion rate and age) should decrease exponentially and join  
548 the two measured  $^{36}\text{Cl}$  concentration points. To construct this profile, we (1) made  
549 different age hypotheses for CRT I<sub>1</sub>, (2) used the  $^{36}\text{Cl}$  concentration measured at the

550 surface ( $C_{m_{\text{surface}}}$ ) to start the profile, (3) set the denudation rate automatically by  
551 combining the measured  $^{36}\text{Cl}$  concentration at the surface ( $C_{m_{\text{surface}}}$ ) with the chosen  
552 hypothetical age, and (4) set a minimum and a maximum of reef porosity from 0% (i.e.,  
553 density  $2.5 \text{ g cm}^{-3}$ ) to 50 % (i.e., a density of  $1.25 \text{ g cm}^{-3}$ ) (e.g., Smith, 1983). We test  
554 the ages proposed by Pirazzoli et al. (1991; 1993): MIS 5e, c and a, as well as an  
555 extremely old age, i.e., 1.5 Ma, to test a steady state hypothesis (Schimmelpfennig et  
556 al., 2009).

557

558 In any case, it is not possible to join the two  $^{36}\text{Cl}$  concentrations measured by the  
559 theoretical  $^{36}\text{Cl}$  concentration profiles (Fig. 7). Regardless of the scenario, the  $2.5 \pm 0.1$   
560 m deep sample exhibits a  $^{36}\text{Cl}$  concentration higher than its theoretical estimate (Fig.  
561 7). The only exception is observed with a 50% porosity and the age of the drilled unit  
562 estimated at 1.5 Ma. However, this age is too old compared to the dating done by  
563 previous authors on the studied CRT (Pirazzoli et al., 1991; 1993; Bard et al., 1996).  
564 The only way to explain the high  $^{36}\text{Cl}$  concentration of the sample at  $2.5 \pm 0.1$  m is that  
565 this reefal limestone unit has been exposed to cosmic radiation before an overlapping  
566 unit was emplaced, i.e., in a later stage of reoccupation. It follows that the borehole  
567 goes through two reefal limestone units, the upper one being thinner than 2.5 m.

568

569 We thus hypothesize that this difference in the  $^{36}\text{Cl}$  concentrations measured has been  
570 acquired on the temporarily emerged surface of the CRT between two successive  
571 highstands. We then calculate exposure times before overlapping with  $\Delta c$  (i.e.,  
572 difference between the measured and theoretical  $^{36}\text{Cl}$  concentration at a depth of 2.5  
573 m; Table 4) according to possible ages of MIS 5a, MIS 5c and MIS 5e for the surface  
574 unit ( $Ed_{\Delta c}$  in Table 4; Pirazzoli et al., 1991; 1993; Bard et al., 1996). These values

575 correspond to minimum exposure time because after overlapping, the  $^{36}\text{Cl}$   
576 concentration decreases with isotopic decay. Considering the ages of MIS 5e, 5c and  
577 5a, which are  $122 \pm 6$  ka,  $100 \pm 5$  ka, and  $82 \pm 3$  ka, respectively (Cutler et al., 2003),  
578 the time intervals between isotopic stages 5e-5c, 5c-5a and 5e-5a are  $22 \pm 11$  ka,  $18$   
579  $\pm 8$  ka, and  $40 \pm 9$  ka, respectively. For the zero-porosity hypothesis, the calculated  
580 exposure times before overlapping ( $13.8 \pm 1.3$  ka,  $12.5 \pm 1.2$  ka, and  $11.0 \pm 1.2$  ka) are  
581 equivalent to the time intervals between two successive substages of MIS 5 (Table 4).  
582 Consequently, our data argue that the borehole intersected two units that could be  
583 associated to the two of the three relative highstands of the last interglacial: MIS 5a  
584 and 5c, or MIS 5c and 5e (Table 4; Fig. 7).

585

586 We conclude that the  $^{36}\text{Cl}$  borehole method confirms previous observations deduced  
587 from  $^{230}\text{Th}/\text{U}$  ages (Pirazzoli et al., 1991; 1993; Bard et al., 1996), and that CRT I<sub>1</sub> is  
588 composite and was built during at least two successive highstands of the last  
589 interglacial.

590

### 591 **5.1.2. Evidence for marine erosion and constructive reoccupation**

592

593 Combining cosmogenic nuclide analyses and  $^{230}\text{Th}/\text{U}$  dating on reef samples collected  
594 near sea level allows to discuss the hypothesis of Pirazzoli et al., (1993) that reef  
595 reoccupation is associated with marine erosion (Fig. 1A). Our two samples from CRT  
596 H, one at the base (SUM18-47,  $0.30 \pm 0.03 \cdot 10^5$  atoms  $\text{g}^{-1}$  rock) and the other at the  
597 top of the modern sea cliff (SUM18-46,  $0.38 \pm 0.04 \cdot 10^5$  atoms  $\text{g}^{-1}$  rock), give similar  
598 low  $^{36}\text{Cl}$  concentrations (Table 2). If sample SUM18-47 had been recently exposed by  
599 sea cliff retreat, its  $^{36}\text{Cl}$  concentration would be much lower (e.g., Regard et al., 2012).

600 Therefore, the two samples at the top and the base of the modern sea cliff likely  
601 experienced the same erosive history over the time interval resolved by the  $^{36}\text{Cl}$   
602 method ( $\sim 1.5$  ka). In view of their location close to sea level and the high denudation  
603 rates calculated from the top of the modern sea cliff (average of  $430 \pm 214$  mm  $\text{ka}^{-1}$ ),  
604 the erosion process is most likely marine. The efficiency of marine erosion has already  
605 been demonstrated by numerous studies, in particular using cosmonuclides (Gibb,  
606 1978; Spencer, 1985; Stephenson and Kirk, 1998; Brown et al., 2003; Raimbault et al.,  
607 2018). In Grand Cayman Island, the average marine erosion rate affecting reef  
608 shielded coasts is  $450$  mm  $\text{ka}^{-1}$  (Spencer, 1985), which is in agreement with our  
609 denudation rate values. However, denudation rates affecting the active sea cliff at  
610 Cape Laundi were calculated on small length (sample of few centimeters) and time  
611 (age hypothesis of few thousand years) scales. It may reflect the stochastic nature of  
612 erosion, i.e., the detachment of a small block that can generate a large difference on  
613 the calculated denudation rates. Such efficient erosion at sea level during a relatively  
614 short period of time can be caused by extreme events, such as storms, cyclones, or  
615 tsunamis (Anderson et al., 1999). Consequently, a comparison with denudation rates  
616 averaged over much larger temporal and spatial scales may be misleading.

617

618 Whatever the uplift rate or the value of the glacial isostatic adjustment, the location of  
619 the samples dated at  $5.45 \pm 0.02$  ka and  $2.13 \pm 0.01$  ka at the same altitude and a few  
620 metres apart can only be explained by erosion and reoccupation. In addition, we have  
621 observed fossil tidal pools on the CRT H surface (Fig. 5I), where the coral dated as  
622  $2.13 \pm 0.01$  ka was sampled, which allows us to specify the reoccupation mode.  
623 Therefore, we interpret the coral dated at  $2.13 \pm 0.01$  ka (SUM17-13) as a coral-colony  
624 that settled on the top surface of the active sea cliff in fossil tidal pools fed by seawater

625 during high tides or storms, as observed elsewhere (e.g., Hoeksema, 2012). As such,  
626 we conclude that the constructive reoccupation affected the CRT H during the Mid-  
627 Holocene with a partial immersion of the reef platform.

628

### 629 **5.1.3. Argument of the abandonment of the main CRT (I) in a single** 630 **eustatic event.**

631

632 Cosmogenic nuclide data also inform us about the processes of CRT abandonment  
633 during regression. CRT I is not old enough to have reached cosmogenic steady state.  
634 However,  $^{36}\text{Cl}$  concentrations measured on the main CRT I ( $I_1$ ,  $I_2$ ) are uniform (Table  
635 2, Fig. 6), suggesting a similar exposure time to radiation for the whole surface of CRT  
636 I. Thus, the abandonment of CRT I surface most probably corresponds to a discrete,  
637 single event, during regression after the last interglacial highstand.

638

## 639 **5.2. Continental denudation of CRTs**

### 640 **5.2.1. Comparison with global trends of carbonate denudation** 641 **rates**

642

643 In previous studies, continental denudation of reef carbonate landforms has been  
644 quantified by taking direct *in situ* measurements, for example,  $^{36}\text{Cl}$  concentrations (Lal  
645 et al., 2005) as well as micro-erosion (e.g., Trudgill, 1976; 1979). Each method is  
646 representative of a given period of time on which the calculated denudation rates are  
647 integrated. For the  $^{36}\text{Cl}$  method, this period is between  $10^3$  to  $10^5$  years. In contrast,  
648 the micro-erosion method covers periods of only one to two years (e.g., Trudgill, 1976;  
649 Spencer, 1985).

650

651 Denudation rates at Cap Laundi (average of  $14.7 \pm 8.3 \text{ mm ka}^{-1}$ ), where precipitation  
652 rates are  $\sim 1000 \text{ mm a}^{-1}$ , are lower than those of tropical sites with higher rainfall ( $>$   
653  $2000 \text{ mm a}^{-1}$ ), such as in Papua New Guinea (denudation rate of  $\sim 150 \text{ mm ka}^{-1}$ ,  
654 Vasconcelos and Stone, 2000), higher than those obtained in arid to hyper-arid zones  
655 (denudation rate of from 1 to  $3 \text{ mm ka}^{-1}$ , Ryb et al., 2014) and similar to those derived  
656 with the same method ( $^{36}\text{Cl}$  concentration) on the same features (upper Pleistocene  
657 CRTs) at locations with the same mean annual precipitation rates ( $1200\text{-}1500 \text{ mm a}^{-1}$   
658 in Rendezvous Hill, Barbados and  $\sim 915 \text{ mm a}^{-1}$  in Isla Mona, Puerto Rico). Denudation  
659 rates range from 7 to  $118 \text{ mm ka}^{-1}$  on the Rendezvous Hill and from 26 to  $61 \text{ mm ka}^{-1}$   
660 at Isla Mona (Lal et al., 2005). Trudgill (1976; 1979) obtained similar denudation rates  
661 ( $9\text{-}62 \text{ mm ka}^{-1}$ ) in Aldabra atoll (Seychelles archipelago), that receives comparable  
662 rainfalls (Shekeine et al., 2015). Thus, denudation rates calculated at Cape Laundi are  
663 consistent with the global correlation between rainfall and denudation rates determined  
664 by the *in situ*  $^{36}\text{Cl}$  method on carbonate flat surfaces (Ryb et al., 2014; Levenson et al.,  
665 2017). These continental denudation rates imply a surface stripping rate of 0.7 to 2.3  
666 m per glacial/interglacial cycle. If the younger reef unit are thin as suggested by the  
667 drilling results, this stripping is sufficient to reveal older reef units at the surface (Fig.  
668 1C).

669

## 670 **5.2.2. Heterogeneous variations of denudation rates across the**

### 671 **sequence as well as individual CRT**

672

673 Denudation rates (i.e.,  $^{36}\text{Cl}$  concentrations) vary across the sequence, as well as within  
674 each CRT. In the following, we propose that this is mainly due to the sampling bias

675 related to the roughness of the carbonate surfaces and the staircase morphology of  
676 the sequence.

677

#### 678 **5.2.2.1. Roughness versus $^{36}\text{Cl}$ concentrations**

679

680 Over time, aerial dissolution forms larger and larger dissolution pits, amplifying the  
681 roughness of the CRT (Figs. 5A; 5B; 5F; 5G). Thus, at Cape Laundi, the older the CRT,  
682 the rougher it is (Figs. 5A; 5B; 5F; 5G). The roughness of all CRTs is in the order of  
683 decimeters (Fig. 5B). We also observed a coastal karren-type epikarstification (e.g.,  
684 Lundberg, 2019). This process induces a detachment of 10 to 50 cm thick blocks from  
685 the CRT surface (Figs. 5B; 8A; 8B). The types of corals, sediments, and stage of  
686 cementation produce distinctive layers of limestone rocks in fossilized reefs (James  
687 and Macintyre, 1985). The layering of the paleo-reef could therefore play an important  
688 role in the development of these karstic forms (Figs. 8A; 8B).

689

690 Block detachment could produce a change of  $^{36}\text{Cl}$  concentrations over the CRTs  
691 surfaces with low values on recently dismantled zones. The following goal is to get an  
692 independent estimate of the typical block size removed by these karstification  
693 processes using our  $^{36}\text{Cl}$  data. We selected two pairs of surface samples from the flat  
694 part of the same CRT that yield different  $^{36}\text{Cl}$  concentrations (SUM18-21/SUM16-4 and  
695 SUM18-20/SUM16-10) and we hypothesized that the difference in  $^{36}\text{Cl}$  concentration  
696 values for each pair is related to the dismantling of the surface blocks. The pairs are  
697 located on CRTs I<sub>2</sub> and II<sub>4</sub>, respectively (Fig. 8C). We calculate the theoretical depth  
698 profile of  $^{36}\text{Cl}$  concentrations from the CRTs age inferred by Pirazzoli et al. (1991; 1993)  
699 combined with the measured  $^{36}\text{Cl}$  concentration for the most concentrated surface

700 sample (Fig. 8C). To quantify the stripped thickness required to achieve the lowest  $^{36}\text{Cl}$   
701 concentration of each pair, we projected this concentration onto the calculated  
702 theoretical depth profile of  $^{36}\text{Cl}$  concentrations (Fig. 8C). We obtained stripped  
703 thicknesses of ~30 cm and ~82 cm for CRTs I<sub>2</sub> and II<sub>4</sub>, respectively (Fig. 8C). These  
704 results are consistent with the natural roughness observed and the height generated  
705 by the detachment of a block (Figs. 5B; 8A). Thus, the difference in  $^{36}\text{Cl}$  concentration  
706 between each pair of samples can be attributed to the removal of a single block.  
707 Variations in  $^{36}\text{Cl}$  concentration on the same CRT can be explained by the spatial  
708 variations of the degradation of the initial CRT surface. The greater the thickness of  
709 the removed blocks, the greater the variations in  $^{36}\text{Cl}$  concentration at the surface  
710 related to its dismantling will be (Figs. 8B; 8C). Such spatial variations in denudation  
711 rates imply that it is impossible to accurately date, with the analysis cosmogenic  $^{36}\text{Cl}$   
712 concentrations, a CRT that has not yet reached the steady state (such as CRT I)  
713 because it requires having a uniform value of this parameter all along the CRT.  
714 Besides, these results suggest that on a given polycyclic CRT, the continental  
715 denudation can partially strip the thin superficial layer of a young fossil coral reef and  
716 exhume older corals in several places.

717

#### 718 **5.2.2.2. CRT morphology versus $^{36}\text{Cl}$ concentrations**

719

720 When samples are divided according to their distribution on the CRT (i.e., inner edge,  
721 terrace main surface, and distal edge) (Table 3), denudation rates reveal different  
722 averages, with the highest values for the distal edges (Fig. 9). Although the non-  
723 parametric statistical test (Kruskal-Wallis test) reveals that there is no significant  
724 difference in denudation rates as a function of the morphological location of the sample

725 analyzed ( $P_{\text{value}} = 0.26$ ), we consider that the distal edges are the most sensitive to  
726 continental denudation because of their position at the top of the slope (Figs. 2; 6). In  
727 this case, distal edges could be faster dissolved by diffusion between the fossil sea cliff  
728 and fossil reef flat, and regressive erosion associated with runoff on the cliff. The flat  
729 geometry of the CRT main surfaces prevents diffusion and runoff that could increase  
730 the denudation rate. Furthermore, there may be a change in porosity between the main  
731 surface and the distal edge of CRTs that may cause the dissolution rate to vary  
732 spatially. The main surfaces of CRTs, considered a paleo lagoon (Cabioch, 2011), can  
733 be then partly formed by the compaction and deposition of marine cements (Figs. 5C;  
734 5D; 5E; Hopley, 2011), which reduces the porosity of the framework. The distal edges  
735 of the CRTs, considered as the paleo reef crests (e.g., Pirazzoli et al., 1991; Rovere et  
736 al., 2016), therefore appear to have a higher porosity than the main surfaces. The  
737 greater the porosity, the more it allows the infiltration of meteoric water, accelerating  
738 chemical dissolution and therefore potentially the denudation rate. Which in turn  
739 explains the high roughness of the distal edges compared to other parts of the CRTs  
740 (Fig. 5G).

741

### 742 **5.2.2.3. Water, sands cover and soil formation on CRT**

#### 743 **versus $^{36}\text{Cl}$ concentration**

744

745 CRTs may be flooded during the subsequent interglacial substages if uplift rates are  
746 low or if marine erosion lowers the CRT (Fig. 1). This process could play a role in  
747 shielding and affect the production of  $^{36}\text{Cl}$  on CRTs older than Holocene. However, the  
748 integration time of the denudation rates calculated here (i.e.,  $61.7 \pm 49.6$  ka in average)  
749 is too short to have recorded several highstands.

750

751 Besides, CRTs may also be covered by sand and debris during and after periods of  
752 intense marine erosion. Indeed, we observed that CRT I<sub>1</sub> surface is covered by  
753 centimeter-scale remnants of a sandstone layer including coral rubbles (Fig. 5E). The  
754 process that forms this layer may be related to marine diagenetic cementation (Rasser  
755 and Riegl, 2002). Storms are the natural events that generally explain the formation  
756 and deposition of these layers (e.g., Scoffin, 1993; Bourrouilh-Le Jan, 1998; Blanchon  
757 et al. 1997; Rasser and Riegl, 2002). Yet, they are also common features in sites  
758 characterised by gently sloping, pre-existing surfaces (i.e., composite CRTs in our  
759 study site) and medium wave energy (Cabiocch et al., 1995). These sand patches are  
760 widely scattered on the lower CRTs and are absent on the upper CRTs due to  
761 continental denudation. They must have been removed during the CRT emergence by  
762 marine erosion (only a few pieces remain; Figs. 5C; 5E) and by continental denudation  
763 after the reef emersion. With a continental denudation rate of  $14.7 \pm 8.3 \text{ mm ka}^{-1}$  on  
764 average, it takes only ~7000 years to strip off a few tens of centimeters. Besides, this  
765 thickness is too small to significantly affect the denudation rates and to be distinguished  
766 from the stripping effect.

767

768 Our field observations have shown that soil is almost non-existent on the lowest CRTs  
769 (Figs. 5D; 5E) and the soil on CRTs above CRT III is very thin (a few millimeters to  
770 centimeters) and only allows the formation of vegetation of steppe moor (Figs. 5A; 5B;  
771 5D; 5F; 5G). The relatively dry climate of the Cape Laundi region (e.g., Prasetia et al.,  
772 2013) may be the cause of the lack of thick soil, which can affect the production of <sup>36</sup>Cl.  
773 But despite this arid climate, the contribution of volcanic ash from the Sunda-Banda  
774 arc or of Australian dust could favour the development of soil. This has already been

775 observed in Barbados, where the parent materials of the soils on uplifted CRTs are  
776 Sahara dust and volcanic ash from the Lesser Antilles Island arc (Muhs, 2001). Similar  
777 examples have been reported in Taiwan (Liew and Hsieh, 2000) as well as in Liuchiu  
778 Island (Cheng et al., 2011). It remains an open question whether deforestation (e.g.,  
779 Orr et al, 2012) and agricultural burning (e.g., Russell-Smith et al., 2007) could have  
780 removed the soil formed over time, despite the low runoff induced by the horizontality  
781 of the surfaces of the CRT. We have not observed any soil trapped and preserved in  
782 the dissolution features (i.e., coastal karren; Lundberg, 2019) or superficial cracks of  
783 the CRTs to testify to its previous existence. Over time, soil forms from the *in situ*  
784 weathering of the initial surface of the CRT and thickens. An older CRT should  
785 therefore have a thicker soil, a more weathered surface and be more protected from  
786 cosmic rays (shielding action) than a more recent CRT. Thus, we should have  
787 observed a decrease in the  $^{36}\text{Cl}$  concentration with the age of the CRT with former  
788 thick soil now gone. We have not observed such a trend in our data. Therefore, we  
789 have no evidence of the influence of soils on the  $^{36}\text{Cl}$  production in the CRTs at Cape  
790 Laundi.

791

## 792 **6. Conclusions**

793

794 At Cape Laundi, previous studies (Pirazzoli et al., 1991; 1993; Bard et al., 1996) have  
795 identified age discrepancies on CRTs. We disentangled the roles of continental  
796 denudation, coastal erosion, and marine reoccupation in the promiscuity of diachron  
797 coral colonies on the same CRT surface. The  $^{36}\text{Cl}$  concentrations of 34 surface  
798 limestone samples taken from different morphological zones of this CRTs sequence  
799 allowed us to calculate continental denudation rates, ranging from  $2.5 \pm 0.3$  to  $37.1 \pm$

800 0.1 mm ka<sup>-1</sup> (14.7 ± 8.3 mm ka<sup>-1</sup> on average). The combined analysis of <sup>230</sup>Th/U ages  
801 and cosmogenic <sup>36</sup>Cl concentrations of surface and depth samples in both the distal  
802 and proximal part of the lowermost CRT suggest that this CRT is composite and  
803 records a polycyclic history with alternating construction and erosion phases during the  
804 eustatic sea level variations of the last interglacial highstands (MIS 5e, 5c, and 5a) and  
805 during the Mid-Holocene. Our results also highlight 1) significant spatial variability in  
806 denudation rates, probably related to roughness and morphological zoning of CRTs,  
807 which could bring coral colonies of different ages to the surface depending on the  
808 efficiency of continental denudation, and 2) higher denudation rates affecting the distal  
809 edges of CRTs than in other parts of the landform. Eventually, we stress that such  
810 erosion processes, suggested since a long time but rarely discussed in the literature,  
811 should be systematically taken into account when establishing the morphostratigraphy  
812 of emerged coral reef terrace sequences.

813

## 814 **Acknowledgements**

815

816 This work was supported by public funds received in the framework of GEOSUD, a  
817 project (ANR-10-EQPX-20 and ANR-10-LABX-19-01, Labex Mer, CLIMORESO, C.  
818 Authemayou) of the program "Investissements d'Avenir" managed by the French  
819 National Research Agency, the INSU Tellus Syter program (SECOMAS, C.  
820 Authemayou) and the CNES TOSCA program (CETTROPICO, C. Authemayou). We  
821 thank the German Aerospace Center for providing us the TanDEM-X data for our study  
822 zone. We thank the State Ministry of Research and Technology of Indonesia "RISTEK"  
823 that allowed us to conduct the field trip to Sumba (research permit  
824 680/FRP/E5/Dit.KI/IV/2017). We also thank the National Geographic Explorer grant

825 (no CP 087R 17) to support the Indonesian researchers (Sri Yudawati Cahyarini, Vera  
826 Christanti Agusta, and Danny Hilman Natawidjaja). Denis Scholz is thankful to the DFG  
827 for funding (SCHO 1274/11-1 and INST 247/889-1 FUGG). We thank Gilles Brocard  
828 for his help with karstic terminology. Finally, we thank 3 anonymous reviewers for  
829 fruitful discussions on former versions of this manuscript.

830

### 831 **References cited**

832

833 1. Abdullah, C. I., Rampnoux, J. P., Bellon, H., Maury, R. C., & Soeria-Atmadja, R.  
834 (2000). The evolution of Sumba Island (Indonesia) revisited in the light of new  
835 data on the geochronology and geochemistry of the magmatic rocks. *Journal of*  
836 *Asian Earth Sciences*, 18(5), 533-546.

837

838 2. Alfonso-Sosa, E. (2016). Tidal mixing in the Sumba Strait and internal wave  
839 activity detected during strong semidiurnal forcing.

840

841 3. Andersen, M. B., Stirling, C. H., Zimmermann, B., & Halliday, A. N. (2010).  
842 Precise determination of the open ocean  $^{234}\text{U}/^{238}\text{U}$  composition.  
843 *Geochemistry, Geophysics, Geosystems*, 11(12).

844

845 4. Anderson, R. S., Densmore, A. L., & Ellis, M. A. (1999). The generation and  
846 degradation of marine terraces. *Basin Research*, 11(1), 7-20.

847

848 5. Authemayou, C., Brocard, G., Delcaillau, B., Molliex, S. p., Pedoja, K., Husson,  
849 L., et al. (2018). Unraveling the roles of asymmetric uplift, normal faulting and

- 850 groundwater flow to drainage rearrangement in an emerging karstic landscape.  
851 Earth Surface Processes and Landforms, 43(9), 1885-1898.  
852
- 853 **6.** Bard, E., Jouannic, C., Hamelin, B., Pirazzoli, P., Arnold, M., Faure, G., et al.  
854 (1996). Pleistocene sea levels and tectonic uplift based on dating of corals from  
855 Sumba Island, Indonesia. Geophysical Research Letters, 23(12), 1473-1476.  
856
- 857 **7.** Bierman, P. R. (1994). Using in situ produced cosmogenic isotopes to estimate  
858 rates of landscape evolution: A review from the geomorphic perspective.  
859 Journal of Geophysical Research: Solid Earth, 99(B7), 13885-13896.  
860
- 861 **8.** Blanchon, P., Jones, B., & Kalbfleisch, W. (1997). Anatomy of a fringing reef  
862 around Grand Cayman; storm rubble, not coral framework. Journal of  
863 Sedimentary Research, 67(1), 1-16.  
864
- 865 **9.** Bourrouilh-Le Jan, F. G. (1998). The role of high-energy events (hurricanes  
866 and/or tsunamis) in the sedimentation, diagenesis and karst initiation of tropical  
867 shallow water carbonate platforms and atolls. Sedimentary Geology, 118(1-4),  
868 3-36.  
869
- 870 **10.** Braucher, R., Del Castillo, P., Siame, L., Hidy, A. J., & Bourles, D. L. (2009).  
871 Determination of both exposure time and denudation rate from an in situ-  
872 produced <sup>10</sup>Be depth profile: a mathematical proof of uniqueness. Model  
873 sensitivity and applications to natural cases. Quaternary Geochronology, 4(1),  
874 56-67.

875

876 **11.**Braucher, R., Merchel, S., Borgomano, J., & Bourlès, D. L. (2011). Production  
877 of cosmogenic radionuclides at great depth: a multi element approach. Earth  
878 and Planetary Science Letters, 309(1-2), 1-9.

879

880 **12.**Brown, J., Jorgenson, M. T., Smith, O. P., & Lee, W. (2003). Long-term rates of  
881 coastal erosion and carbon input, Elson Lagoon, Barrow, Alaska. Paper  
882 presented at the Eighth International Conference on Permafrost.

883

884 **13.**Butt, T., Russell, P., & Grigg, R. (2004). Surf science: An introduction to waves  
885 for surfing: University of Hawaii Press Honolulu.

886

887 **14.**Cabioch, G., Montaggioni, L. F., & Faure, G. (1995). Holocene initiation and  
888 development of New Caledonian fringing reefs, SW Pacific. Coral Reefs, 14(3),  
889 131-140.

890

891 **15.**Cabioch, G. (2011). Emerged reefs. Encyclopedia of Modern Coral Reefs:  
892 Structure, Form and Process, 373-380.

893

894 **16.**Chappell, J. (1974). Geology of coral terraces, Huon Peninsula, New Guinea: a  
895 study of Quaternary tectonic movements and sea-level changes. Geological  
896 Society of America Bulletin, 85(4), 553-570.

897

898 **17.**Cheng, C.-H., Jien, S.-H., Tsai, H., & Hseu, Z.-Y. (2011). Geomorphological and  
899 paleoclimatic implications of soil development from siliceous materials on the

900 coral-reef terraces of Liuchiu Island in southern Taiwan. Soil science and plant  
901 nutrition, 57(1), 114-127.

902

903 **18.**Codilean, A. T. (2006). Calculation of the cosmogenic nuclide production  
904 topographic shielding scaling factor for large areas using DEMs. Earth Surface  
905 Processes and Landforms, 31(6), 785-794.

906

907 **19.**Colas, A., & Sutherland, B. (2001). The world stormrider guide: Low Pressure.

908

909 **20.**Crosby, W. O. (1883). Elevated coral reefs of cuba. Journal of Natural History,  
910 12(70), 283-284.

911

912 **21.**Cutler, K. B., Edwards, R. L., Taylor, F. W., Cheng, H., Adkins, J., Gallup, C. D.,  
913 et al. (2003). Rapid sea-level fall and deep-ocean temperature change since the  
914 last interglacial period. Earth and Planetary Science Letters, 206(3-4), 253-271.

915

916 **22.**Daly, R. A. (1915). The glacial-control theory of coral reefs.

917

918 **23.**Darwin, C. (1842). The Structure and Distribution of Coral Reefs: Being the First  
919 Part of the Geology of the Voyage of the Beagle... During the Years 1832-1836:  
920 Smith, Elder.

921

922 **24.**Dunai, T. J. (2010). Cosmogenic Nuclides: Principles, concepts and  
923 applications in the Earth surface sciences: Cambridge University Press.

924

- 925       **25.** Fabryka-Martin, J. T. (1988). Production of radionuclides in the earth and their  
926           hydrogeologic significance, with emphasis on chlorine-36 and iodine-129.  
927
- 928       **26.** Fleury, J.-M., Pubellier, M., & de Urreiztieta, M. (2009). Structural expression of  
929           forearc crust uplift due to subducting asperity. *Lithos*, 113(1-2), 318-330.  
930
- 931       **27.** Fortuin, A. R., Van der Werff, W., & Wensink, H. (1997). Neogene basin history  
932           and paleomagnetism of a rifted and inverted forearc region, on- and offshore  
933           Sumba, Eastern Indonesia. *Journal of Asian Earth Sciences*, 15(1), 61-88.  
934
- 935       **28.** Granger, D. E., & Riebe, C. S. (2014). Cosmogenic nuclides in weathering and  
936           erosion.  
937
- 938       **29.** Gibb, J. G. (1978). Rates of coastal erosion and accretion in New Zealand. *New  
939           Zealand journal of marine and freshwater research*, 12(4), 429-456.  
940
- 941       **30.** Gosse, J. C., & Phillips, F. M. (2001). Terrestrial in situ cosmogenic nuclides:  
942           theory and application. *Quaternary Science Reviews*, 20(14), 1475-1560.  
943
- 944       **31.** Haig, D. W. (2012). Palaeobathymetric gradients across Timor during 5.7-3.3  
945           Ma (latest Miocene-Pliocene) and implications for collision uplift.  
946           *Palaeogeography, Palaeoclimatology, Palaeoecology*, 331, 50-59.  
947

- 948 **32.**Hantoro, W. S., Jouannic, C., & Pirazzoli, P. A. (1989). Terrasses coralliennes  
949 quaternaires soulevées dans l'île de Sumba (Indonésie). Photo interprétation  
950 (Paris), 28(1), 17-34.
- 951
- 952 **33.**Hantoro, W. S. (1992). Etude des terrasses récifales Quaternaires soulevées  
953 entre le Détroit de la Sonde et l'île de Timor, Indonésie: mouvements verticaux  
954 de la croûte terrestre et variations du niveau de la mer.
- 955
- 956 **34.**Harris, R. A. (1991). Temporal distribution of strain in the active Banda orogen:  
957 a reconciliation of rival hypotheses. Journal of Southeast Asian Earth Sciences,  
958 6(3-4), 373-386.
- 959
- 960 **35.**Hearty, P. J., & Olson, S. L. (2008). Mega-highstand or megatsunami?  
961 Discussion of McMurtry et al. (Elevated marine deposits in Bermuda record a  
962 late Quaternary megatsunami: Sed. Geol. 200 (2007) 155-165). Sedimentary  
963 Geology, 203(3-4), 307-312.
- 964
- 965 **36.**Hein, A. S., Hulton, N. R. J., Dunai, T. J., Schnabel, C., Kaplan, M. R., Naylor,  
966 M., et al. (2009). Middle Pleistocene glaciation in Patagonia dated by  
967 cosmogenic-nuclide measurements on outwash gravels. Earth and Planetary  
968 Science Letters, 286(1-2), 184-197.
- 969
- 970 **37.**Heisinger, B., Lal, D., Jull, A. J. T., Kubik, P., Ivy-Ochs, S., Neumaier, S., et al.  
971 (2002). Production of selected cosmogenic radionuclides by muons: 1. Fast  
972 muons. Earth and Planetary Science Letters, 200(3-4), 345-355.

973  
974  
975  
976  
977  
978  
979  
980  
981  
982  
983  
984  
985  
986  
987  
988  
989  
990  
991  
992  
993  
994  
995  
996  
997

- 38.**Hibbert, F. D., Rohling, E. J., Dutton, A., Williams, F. H., Chutcharavan, P. M., Zhao, C., et al. (2016). Coral indicators of past sea-level change: A global repository of U-series dated benchmarks. *Quaternary Science Reviews*, 145, 1-56.
- 39.**Hinschberger, F., Malod, J.-A., Réhault, J.-P., Villeneuve, M., Royer, J.-Y., & Burhanuddin, S. (2005). Late Cenozoic geodynamic evolution of eastern Indonesia. *Tectonophysics*, 404(1-2), 91-118.
- 40.**Hoeksema, B. W. (2012). Extreme morphological plasticity enables a free mode of life in *Favia gravida* at Ascension Island (South Atlantic). *Marine Biodiversity*, 42(2), 289-295.
- 41.**Hopley, D. (2011). Density and porosity: influence on reef accretion rates. In: Springer.
- 42.**Husson, L., Pastier, A.-M., Pedoja, K., Elliot, M., Paillard, D., Authemayou, C., et al. (2018). Reef carbonate productivity during Quaternary sea level oscillations. *Geochemistry, Geophysics, Geosystems*, pp. 1148-1164.
- 43.**James, N. P., & Macintyre, I. G. (1985). Carbonate depositional environments- modern and ancient-Part. 1: Reefs-zonation, depositional facies and diagenesis. *Colorado School of Mines Quarterly*, 80(3).

- 998 **44.**Jouannic, C., Hantoro, W. S., Hoang, C. T., Fournier, M., Lafont, R., & Ichtam,  
999 M. L. (1988). Quaternary raised reef terraces at cape Laundi, Sumba,  
1000 Indonesia: geomorphological analysis and first radiometric Th/U and <sup>14</sup>C age  
1001 determinations. Paper presented at the 6th Proceedings International coral reef  
1002 symposium.
- 1003
- 1004 **45.**Kindler, P., Reyss, J.-L., Cazala, C., & Plagnes, V. r. (2007). Discovery of a  
1005 composite reefal terrace of middle and late Pleistocene age in Great Inagua  
1006 Island, Bahamas. Implications for regional tectonics and sea-level history.  
1007 *Sedimentary Geology*, 194(1-2), 141-147.
- 1008
- 1009 **46.**Kummerow, C., Simpson, J., Thiele, O., Barnes, W., Chang, A. T. C., Stocker,  
1010 E., et al. (2000). The status of the Tropical Rainfall Measuring Mission (TRMM)  
1011 after two years in orbit. *Journal of applied meteorology*, 39(12), 1965-1982.
- 1012
- 1013 **47.**Lal, D. (1988). In situ-produced cosmogenic isotopes in terrestrial rocks. *Annual*  
1014 *Review of Earth and Planetary Sciences*, 16(1), 355-388.
- 1015
- 1016 **48.**Lal, D. (1991). Cosmic ray labeling of erosion surfaces: in situ nuclide production  
1017 rates and erosion models. *Earth and Planetary Science Letters*, 104(2-4), 424-  
1018 439.
- 1019
- 1020 **49.**Lal, D., Gallup, C. D., Somayajulu, B. L. K., Vacher, L. c., Caffee, M. W., Jull, A.  
1021 J. T., et al. (2005). Records of cosmogenic radionuclides <sup>10</sup>Be, <sup>26</sup>Al and <sup>36</sup>Cl

- 1022 in corals: First studies on coral erosion rates and potential of dating very old  
1023 corals. *Geochimica et cosmochimica acta*, 69(24), 5717-5728.
- 1024
- 1025 **50.**Levenson, Y., Ryb, U., & Emmanuel, S. (2017). Comparison of field and  
1026 laboratory weathering rates in carbonate rocks from an Eastern Mediterranean  
1027 drainage basin. *Earth and Planetary Science Letters*, 465, 176-183.
- 1028
- 1029 **51.**Liew, P.-M., & Hsieh, M.-L. (2000). Late Holocene (2 ka) sea level, river  
1030 discharge and climate interrelationship in the Taiwan region. *Journal of Asian*  
1031 *Earth Sciences*, 18(4), 499-505.
- 1032
- 1033 **52.**Lundberg, J. (2019). Karren, surface. In *Encyclopedia of Caves* (pp. 600-608):  
1034 Elsevier.
- 1035
- 1036 **53.**Merchel, S., Arnold, M., Aumaître, G., Benedetti, L., Bourlès, D. L., Braucher,  
1037 R., et al. (2008). Towards more precise  $^{10}\text{Be}$  and  $^{36}\text{Cl}$  data from measurements  
1038 at the 10-14 level: influence of sample preparation. *Nuclear instruments and*  
1039 *methods in physics research section B: beam interactions with materials and*  
1040 *atoms*, 266(22), 4921-4926.
- 1041
- 1042 **54.**Muhs, D. R. (2001). Evolution of soils on Quaternary reef terraces of Barbados,  
1043 West Indies. *Quaternary research*, 56(1), 66-78.
- 1044
- 1045 **55.**Murray-Wallace, C. V., & Woodroffe, C. D. (2014). *Quaternary sea-level*  
1046 *changes: a global perspective*: Cambridge University Press.

1047

1048 **56.**Nexer, M., Authemayou, C., Schildgen, T., Hantoro, W. S., Molliex, S.,  
1049 Delcaillau, B., et al. (2015). Evaluation of morphometric proxies for uplift on  
1050 sequences of coral reef terraces: A case study from Sumba Island (Indonesia).  
1051 *Geomorphology*, 241, 145-159.

1052

1053 **57.**Nugroho, H., Harris, R., Lestariya, A. W., & Maruf, B. (2009). Plate boundary  
1054 reorganization in the active Banda Arc-continent collision: Insights from new  
1055 GPS measurements. *Tectonophysics*, 479(1-2), 52-65.

1056

1057 **58.**Obert, J. C., Scholz, D., Felis, T., Brocas, W. M., Jochum, K. P., & Andreae, M.  
1058 O. (2016).  $^{230}\text{Th}/\text{U}$  dating of Last Interglacial brain corals from Bonaire  
1059 (southern Caribbean) using bulk and theca wall material. *Geochimica et*  
1060 *cosmochimica acta*, 178, 20-40.

1061

1062 **59.**Obert, J. C., Scholz, D., Felis, T., Lippold, J., Jochum, K. P., & Andreae, M. O.  
1063 (2019). Improved constraints on open-system processes in fossil reef corals by  
1064 combined Th/U, Pa/U and Ra/Th dating: A case study from Aqaba, Jordan.  
1065 *Geochimica et cosmochimica acta*, 245, 459-478.

1066

1067 **60.** Orr, Y., Schimmer, R., Geerken, R., Castro, A., Taylor, D., & Brokensha, D.  
1068 (2012). Ethno-ecology in the shadow of rain and the light of experience: local  
1069 perceptions of drought and climate change in east Sumba, Indonesia. *Climate*  
1070 *Change and Threatened Communities* [Castro, AP, D. Taylor, and DW  
1071 Brokensha (eds.)]. Practical Action Publishing, Rugby, UK, 175-184.

1072

1073 **61.**Pastier, A. M., Husson, L., Pedoja, K., Bézos, A., Authemayou, C., Arias-Ruiz,  
1074 C., et al. (2019). Genesis and Architecture of Sequences of Quaternary Coral  
1075 Reef Terraces: Insights From Numerical Models. *Geochemistry, Geophysics,*  
1076 *Geosystems.*

1077

1078 **62.**Pedoja, K., Husson, L., Regard, V., Cobbold, P. R., Ostanciaux, E., Johnson,  
1079 M. E., et al. (2011). Relative sea-level fall since the last interglacial stage: are  
1080 coasts uplifting worldwide? *Earth-Science Reviews*, 108(1-2), 1-15.

1081

1082 **63.**Pedoja, K., Husson, L., Johnson, M. E., Melnick, D., Witt, C., Pochat, S. p., et  
1083 al. (2014). Coastal staircase sequences reflecting sea-level oscillations and  
1084 tectonic uplift during the Quaternary and Neogene. *Earth-Science Reviews*,  
1085 132, 13-38.

1086

1087 **64.**Pedoja, K., Husson, L., Bézos, A., Pastier, A.-M., Imran, A. M., Arias-Ruiz, C.,  
1088 et al. (2018). On the long-lasting sequences of coral reef terraces from SE  
1089 Sulawesi (Indonesia): Distribution, formation, and global significance.  
1090 *Quaternary Science Reviews*, 188, 37-57.

1091

1092 **65.**Phillips, F. M., & Plummer, M. A. (1996). CHLOE; a program for interpreting in-  
1093 situ cosmogenic nuclide data for surface exposure dating and erosion studies.  
1094 *Radiocarbon*, 38(1), 98-99.

1095

- 1096 **66.**Phillips, F. M., Stone, W. D., & Fabryka-Martin, J. T. (2001). An improved  
1097 approach to calculating low-energy cosmic-ray neutron fluxes near the  
1098 land/atmosphere interface. *Chemical Geology*, 175(3-4), 689-701.  
1099
- 1100 **67.**Pirazzoli, P. A., Radtke, U., Hantoro, W. S., Jouannic, C., Hoang, C. T., Causse,  
1101 C., et al. (1991). Quaternary raised coral-reef terraces on Sumba Island,  
1102 Indonesia. *Science*, 252(5014), 1834-1836.  
1103
- 1104 **68.**Pirazzoli, P. A., Radtke, U., Hantoro, W. S., Jouannic, C., Hoang, C. T., Causse,  
1105 C., et al. (1993). A one million-year-long sequence of marine terraces on Sumba  
1106 Island, Indonesia. *Marine Geology*, 109(3-4), 221-236.  
1107
- 1108 **69.**Pirazzoli, P. A. (2005). A review of possible eustatic, isostatic and tectonic  
1109 contributions in eight late-Holocene relative sea-level histories from the  
1110 Mediterranean area. *Quaternary Science Reviews*, 24(18-19), 1989-2001.  
1111
- 1112 **70.**Prasetia, R., As-syakur, A. R., & Osawa, T. (2013). Validation of TRMM  
1113 Precipitation Radar satellite data over Indonesian region. *Theoretical and  
1114 applied climatology*, 112(3-4), 575-587.  
1115
- 1116 **71.**Raimbault, C., Duperret, A., Regard, V., Molliex, S., Wyns, R., Authemayou, C.,  
1117 et al. (2018). Quaternary geomorphological evolution of a granitic shore platform  
1118 constrained by in situ <sup>10</sup>Be concentrations, Penmarc'h, SW Brittany, France.  
1119 *Marine Geology*, 395, 33-47.  
1120

- 1121 **72.**Rasser, M., & Riegl, B. (2002). Holocene coral reef rubble and its binding  
1122 agents. *Coral Reefs*, 21(1), 57-72.
- 1123
- 1124 **73.**Regard, V., Dewez, T., Bourles, D. L., Anderson, R. S., Duperret, A., Costa, S.,  
1125 et al. (2012). Late Holocene seacliff retreat recorded by 10Be profiles across a  
1126 coastal platform: Theory and example from the English Channel. *Quaternary*  
1127 *Geochronology*, 11, 87-97.
- 1128
- 1129 **74.**Rovere, A., Raymo, M. E., Vacchi, M., Lorscheid, T., Stocchi, P., Gomez-Pujol,  
1130 L., et al. (2016). The analysis of Last Interglacial (MIS 5e) relative sea-level  
1131 indicators: Reconstructing sea-level in a warmer world. *Earth-Science Reviews*,  
1132 159, 404-427.
- 1133
- 1134 **75.**Rupnik, E., Deseilligny, M. P., Delorme, A., & Klinger, Y. (2016). Refined  
1135 satellite image orientation in the free open-source photogrammetric tools  
1136 Apero/Micmac. *ISPRS Annals of the Photogrammetry, Remote Sensing and*  
1137 *Spatial Information Sciences*, 3, 83.
- 1138
- 1139 **76.**Russell-Smith, J., Djoeroemana, S., Maan, J., & Pandanga, P. (2007). Rural  
1140 livelihoods and burning practices in savanna landscapes of Nusa Tenggara  
1141 Timur, eastern Indonesia. *Human Ecology*, 35(3), 345-359.
- 1142
- 1143 **77.**Ryb, U., Matmon, A., Erel, Y., Haviv, I., Benedetti, L., & Hidy, A. J. (2014). Styles  
1144 and rates of long-term denudation in carbonate terrains under a Mediterranean

1145 to hyper-arid climatic gradient. *Earth and Planetary Science Letters*, 406, 142-  
1146 152.

1147

1148 **78.** Schaller, M., Ehlers, T. A., Blum, J. D., & Kallenberg, M. A. (2009). Quantifying  
1149 glacial moraine age, denudation, and soil mixing with cosmogenic nuclide depth  
1150 profiles. *Journal of Geophysical Research: Earth Surface*, 114(F1).

1151

1152 **79.** Schimmelpfennig, I., Benedetti, L., Finkel, R., Pik, R. I., Blard, P.-H., Bourles,  
1153 D., et al. (2009). Sources of in-situ <sup>36</sup>Cl in basaltic rocks. Implications for  
1154 calibration of production rates. *Quaternary Geochronology*, 4(6), 441-461.

1155

1156 **80.** Schimmelpfennig, I., Benedetti, L., Garreta, V., Pik, R., Blard, P.-H., Burnard,  
1157 P., et al. (2011). Calibration of cosmogenic <sup>36</sup>Cl production rates from Ca and  
1158 K spallation in lava flows from Mt. Etna (38 N, Italy) and Payun Matru (36 S,  
1159 Argentina). *Geochimica et cosmochimica acta*, 75(10), 2611-2632.

1160

1161 **81.** Schimmelpfennig, I., Schaefer, J. M., Putnam, A. E., Koffman, T., Benedetti, L.,  
1162 Ivy-Ochs, S., et al. (2014). <sup>36</sup>Cl production rate from K-spallation in the  
1163 European Alps (Chironico landslide, Switzerland). *Journal of Quaternary  
1164 Science*, 29(5), 407-413.

1165

1166 **82.** Schlagenhauf, A., Gaudemer, Y., Benedetti, L., Manighetti, I., Palumbo, L.,  
1167 Schimmelpfennig, I., et al. (2010). Using in situ Chlorine-36 cosmonuclide to  
1168 recover past earthquake histories on limestone normal fault scarps: a

1169 reappraisal of methodology and interpretations. *Geophysical Journal*  
1170 *International*, 182(1), 36-72.

1171

1172 **83.**Scholz, D., Mangini, A., & Felis, T. (2004). U-series dating of diagenetically  
1173 altered fossil reef corals. *Earth and Planetary Science Letters*, 218(1-2), 163-  
1174 178.

1175

1176 **84.**Schwartz, M. (2006). *Encyclopedia of coastal science*: Springer Science &  
1177 Business Media.

1178

1179 **85.**Scoffin, T. P. (1993). The geological effects of hurricanes on coral reefs and the  
1180 interpretation of storm deposits. *Coral Reefs*, 12(3-4), 203-221.

1181

1182 **86.**Shekeine, J., Turnbull, L. A., Cherubini, P., de Jong, R., Baxter, R., Hansen, D.,  
1183 et al. (2015). Primary productivity and its correlation with rainfall on Aldabra  
1184 Atoll. *Biogeosciences Discussions*, 12(2), 981-1013.

1185

1186 **87.**Simms, A. R. (2021). Last interglacial sea levels within the Gulf of Mexico and  
1187 northwestern Caribbean Sea. *Earth System Science Data*, 13(3), 1419-1439.

1188

1189 **88.**Smith, S. V. (1983). Coral reef calcification. *Perspectives on Coral Reefs*.  
1190 Australian Institute of Marine Science, 240-247.

1191

- 1192 **89.**Speed, R. C., & Cheng, H. (2004). Evolution of marine terraces and sea level in  
1193 the last interglacial, Cave Hill, Barbados. *Geological Society of America Bulletin*,  
1194 116(1-2), 219-232.
- 1195
- 1196 **90.**Spencer, T. (1985). Weathering rates on a Caribbean reef limestone: results  
1197 and implications. *Marine Geology*, 69(1-2), 195-201.
- 1198
- 1199 **91.**Stephenson, W. J., & Kirk, R. M. (1998). Rates and patterns of erosion on inter-  
1200 tidal shore platforms, Kaikoura Peninsula, South Island, New Zealand. *Earth*  
1201 *Surface Processes and Landforms: The Journal of the British Geomorphological*  
1202 *Group*, 23(12), 1071-1085.
- 1203
- 1204 **92.**Stone, J., Allan, G. L., Fifield, L. K., Evans, J. M., & Chivas, A. R. (1994).  
1205 Limestone erosion measurements with cosmogenic chlorine-36 in calcite-  
1206 preliminary results from Australia. *Nuclear instruments and methods in physics*  
1207 *research section B: beam interactions with materials and atoms*, 92(1-4), 311-  
1208 316
- 1209
- 1210 **93.**Stone, J. O., Allan, G. L., Fifield, L. K., & Cresswell, R. G. (1996). Cosmogenic  
1211 chlorine-36 from calcium spallation. *Geochimica et cosmochimica acta*, 60(4),  
1212 679-692.
- 1213
- 1214 **94.**Stone, J. O. H., Evans, J. M., Fifield, L. K., Allan, G. L., & Cresswell, R. G.  
1215 (1998). Cosmogenic chlorine-36 production in calcite by muons. *Geochimica et*  
1216 *cosmochimica acta*, 62(3), 433-454.

1217

1218 **95.** Tate, G. W., McQuarrie, N., Van Hinsbergen, D. J. J., Bakker, R. R., Harris, R.,  
1219 Willett, S., et al. (2014). Resolving spatial heterogeneities in exhumation and  
1220 surface uplift in Timor-Leste: Constraints on deformation processes in young  
1221 orogens. *Tectonics*, 33(6), 1089-1112.

1222

1223 **96.** Thompson, S. B., & Creveling, J. R. (2021). A Global Database of Marine  
1224 Isotope Stage 5a and 5c Marine Terraces and Paleoshoreline Indicators. *Earth*  
1225 *System Science Data Discussions*, 1-32.

1226

1227 **97.** Trudgill, S. T. (1976). The marine erosion of limestones on Aldabra Atoll, Indian  
1228 Ocean. *Zeitschrift für Geomorphologie*, 26, 164-200.

1229

1230 **98.** Trudgill, S. T. (1979). Surface lowering and landform evolution on Aldabra.  
1231 *Philosophical Transactions of the Royal Society of London. B, Biological*  
1232 *Sciences*, 286(1011), 35-45.

1233

1234 **99.** Van der Werff, W. (1995). Cenozoic evolution of the Savu Basin, Indonesia:  
1235 forearc basin response to arc-continent collision. *Marine and Petroleum*  
1236 *Geology*, 12(3), 247-262.

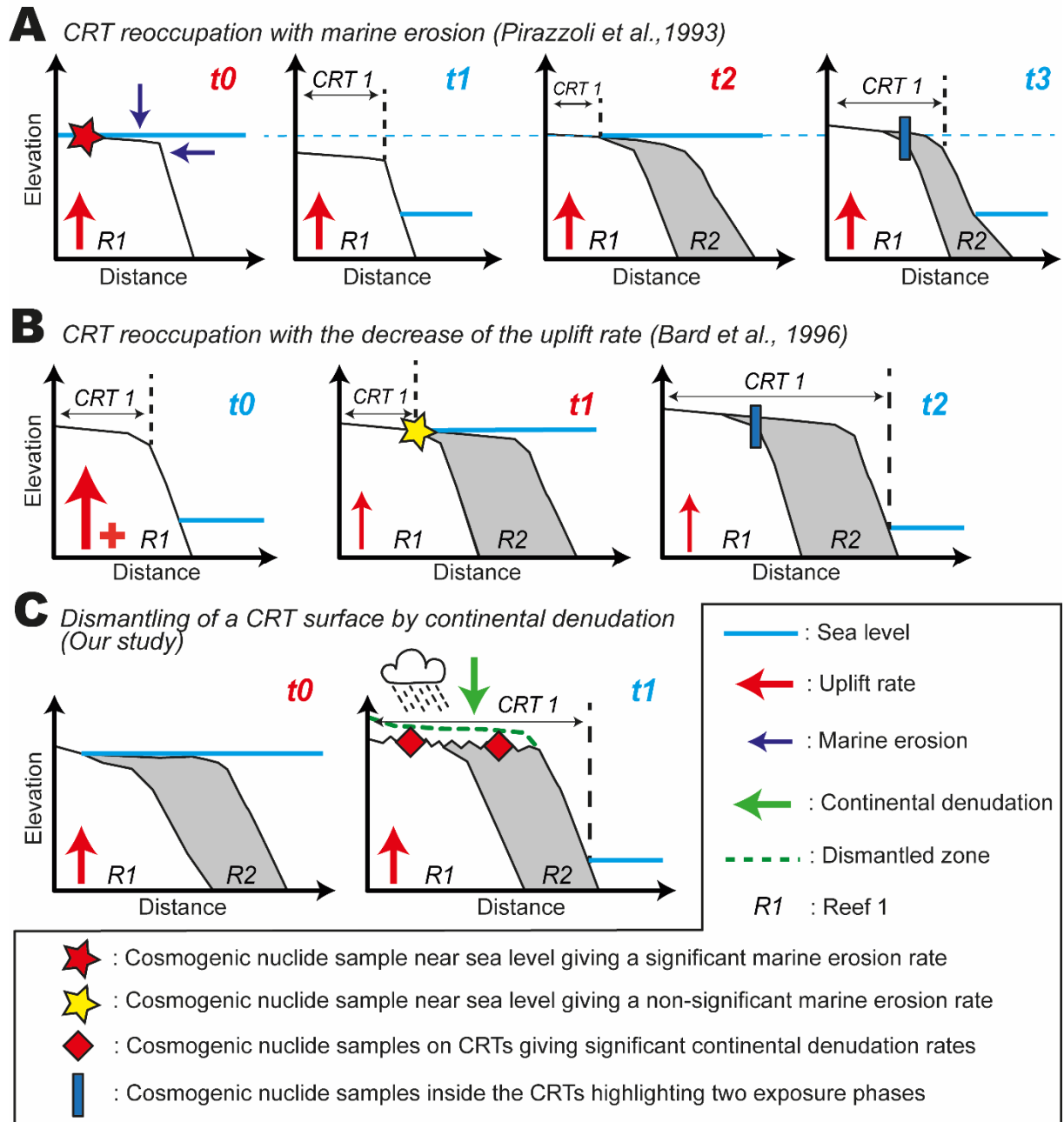
1237

1238 **100.** Vasconcelos, P. M. D., & Stone, J. O. (2000). Studies of geomorphic  
1239 rates and processes with cosmogenic isotopes-examples from Australia.

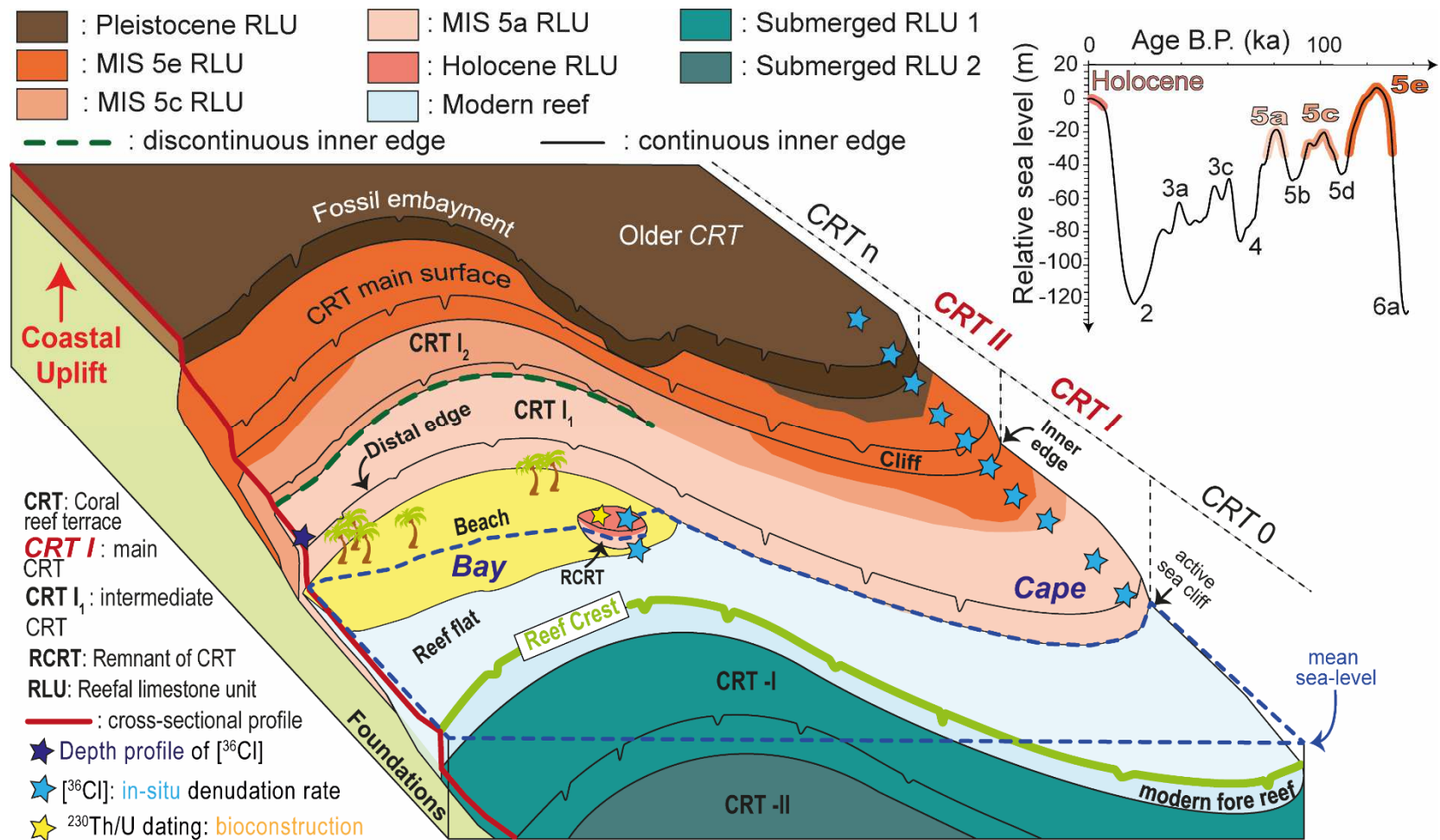
1240

- 1241 **101.** Vermeesch, P. (2007). CosmoCalc: An Excel add-in for cosmogenic  
1242 nuclide calculations. *Geochemistry, Geophysics, Geosystems*, 8(8).  
1243
- 1244 **102.** Von Blanckenburg, F. (2005). The control mechanisms of erosion and  
1245 weathering at basin scale from cosmogenic nuclides in river sediment. *Earth  
1246 and Planetary Science Letters*, 242(3-4), 224-239.  
1247
- 1248 **103.** Von der Borch, C. C., Grady, A. E., Hardjoprawiro, S., Prasetyo, H., &  
1249 Hadiwisastra, S. (1983). Mesozoic and late Tertiary submarine fan sequences  
1250 and their tectonic significance, Sumba, Indonesia. *Sedimentary Geology*, 37(1-  
1251 2), 113-132.  
1252
- 1253 **104.** Waelbroeck, C., Labeyrie, L., Michel, E., Duplessy, J. C., McManus, J.  
1254 F., Lambeck, K., et al. (2002). Sea-level and deep water temperature changes  
1255 derived from benthic foraminifera isotopic records. *Quaternary Science  
1256 Reviews*, 21(1-3), 295-305.  
1257
- 1258 **105.** Yang, Q., Scholz, D., Jochum, K. P., Hoffmann, D. L., Stoll, B., Weis, U.,  
1259 et al. (2015). Lead isotope variability in speleothems-A promising new proxy for  
1260 hydrological change? First results from a stalagmite from western Germany.  
1261 *Chemical Geology*, 396, 143-151.  
1262  
1263  
1264

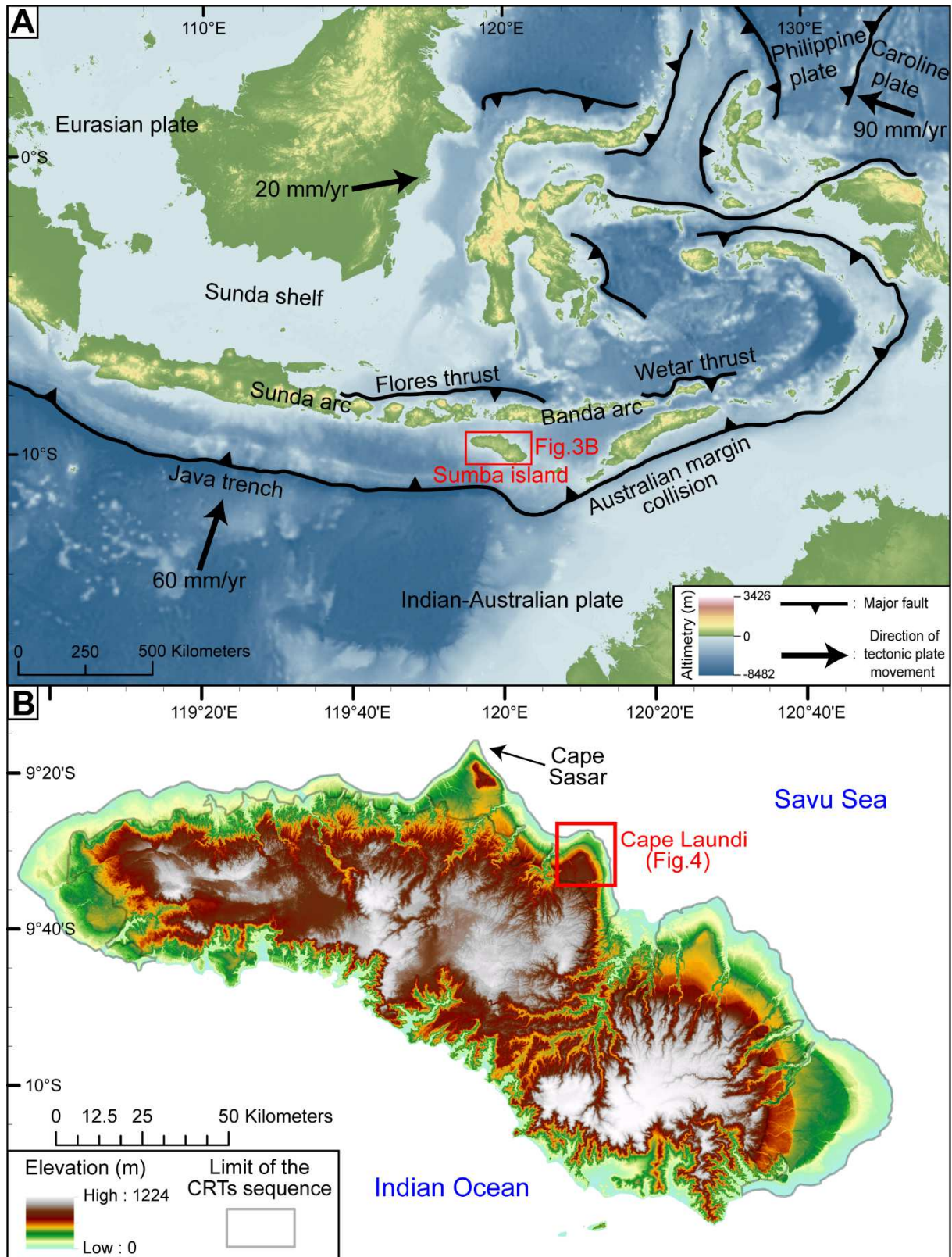
**Figures**



1267 **Fig. 1.** Three hypotheses explaining diachronous ages on the same surface of the  
1268 Cape Laundi CRTs. **A)** Important role of marine erosion in the destruction of the  
1269 emergent CRTs, helping a later reoccupation of these eroded surfaces (Pirazzoli et al.,  
1270 1993). **B)** The decrease in the rate of uplift to a low rate (about  $0.2 \text{ mm a}^{-1}$ ) promotes  
1271 the reoccupation of emergent CRTs without marine erosion (Bard et al., 1996). **C)**  
1272 Alternative hypothesis (this study): continental denudation may partially dismantle  
1273 emergent surfaces, generating a diachronism of these surfaces.  $^{36}\text{Cl}$  cosmogenic  
1274 data on CRT near current sea level reveal the significance of marine erosion (Fig. 1A)  
1275 and continental denudation (Fig. 1C).



1276 **Fig. 2.** Schematic plot of a sequence of coral reef terraces, modified from Pedoja et al. (2018). The blue and yellow stars represent  
 1277 the location of samples collected on the CRT surfaces and intended for analysis in <sup>36</sup>Cl concentration and <sup>230</sup>Th/U dating, respectively.  
 1278 The relative sea level curve is from Waelbroeck et al. (2002).

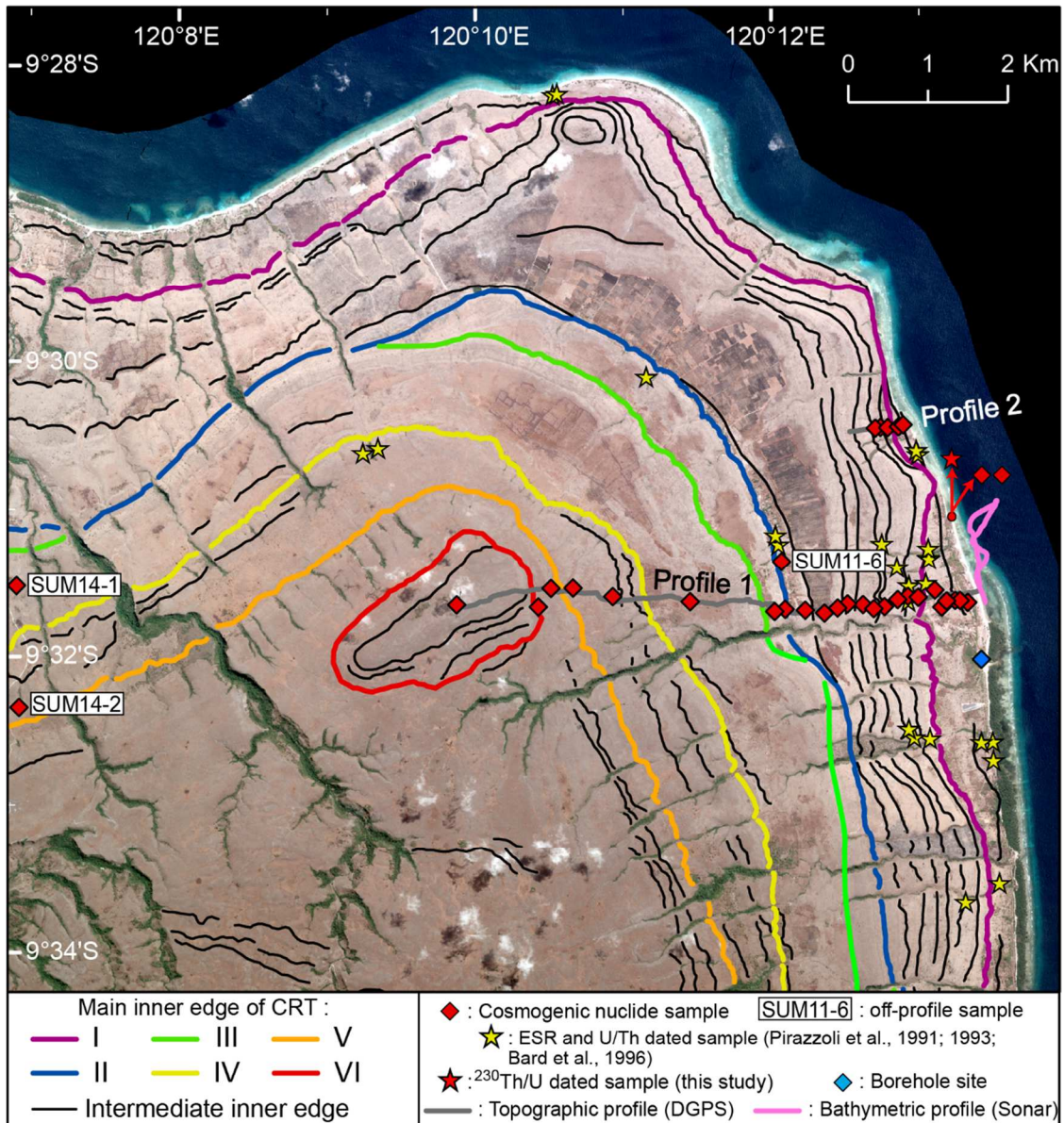


1279 **Fig. 3. A)** Geodynamics of SE Asia and location of Sumba Island (Indonesia). Plate  
 1280 velocities indicated in relation to the Eurasia plate, from Nugroho et al. (2009),  
 1281 elevation data from the Shuttle Radar Topography Mission (SRTM), and bathymetry

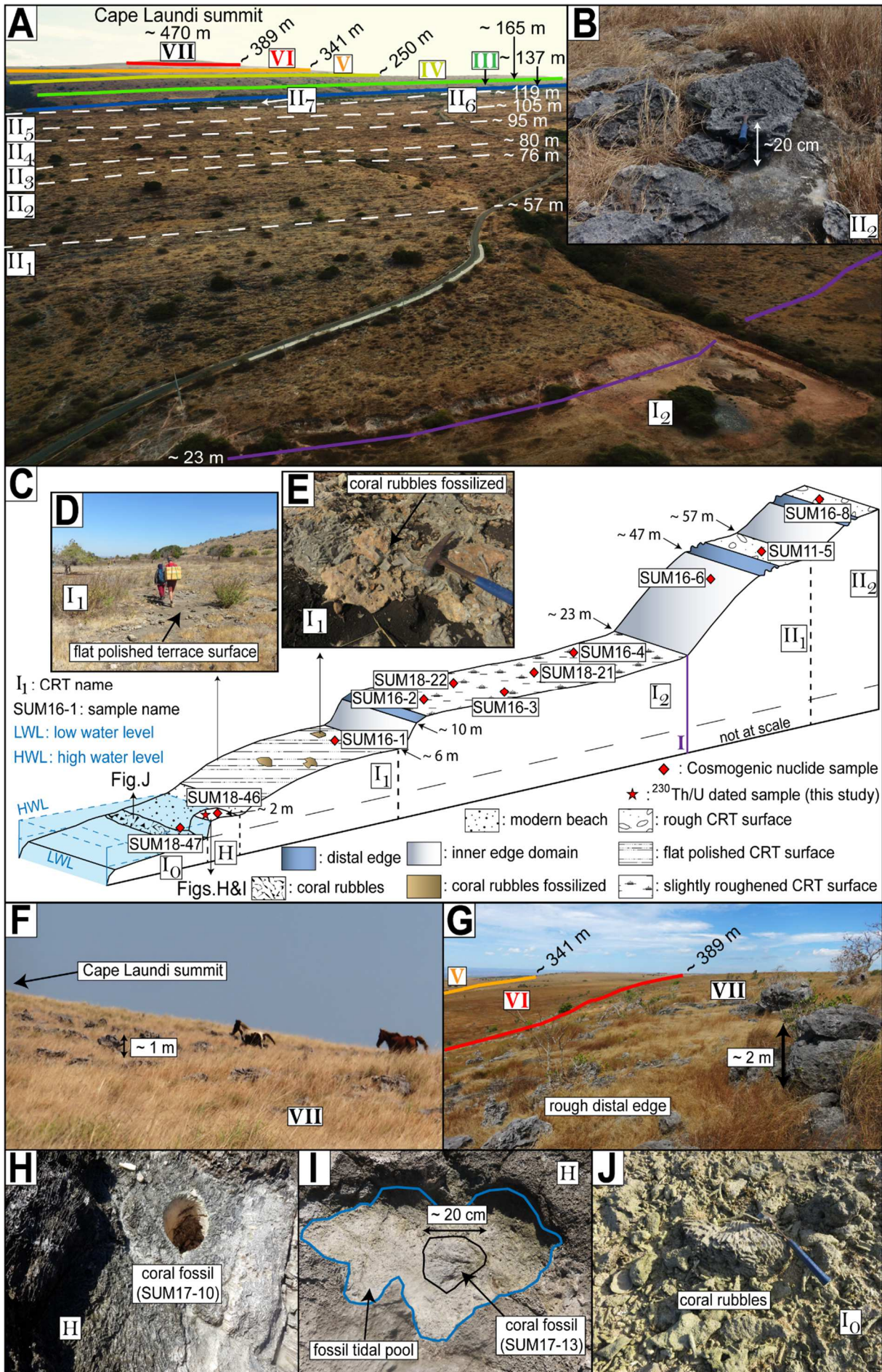
1282 data from the General Bathymetric Chart of Oceans (GEBCO), both at 90 m resolution.

1283 **B)** Digital elevation model (TanDEM-X, 13 m resolution) of Sumba Island.

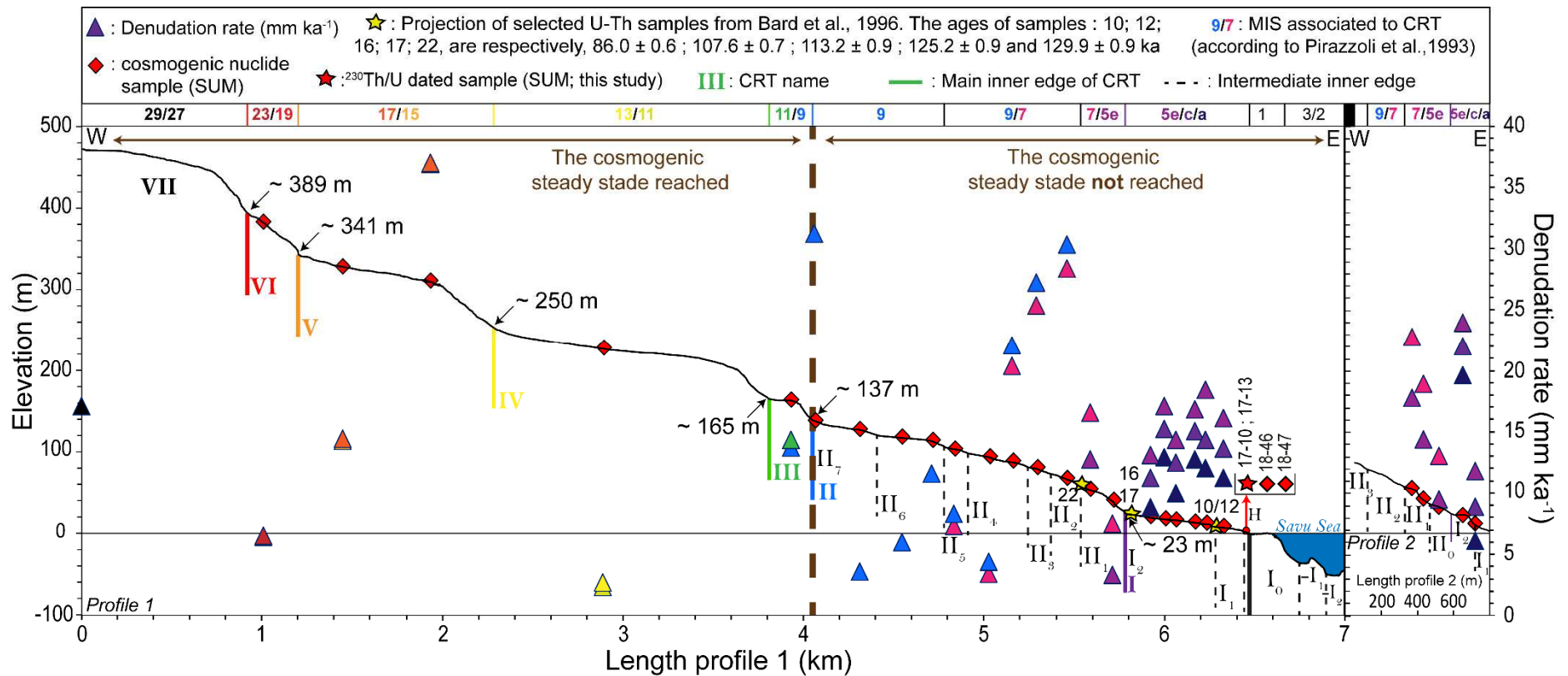
1284



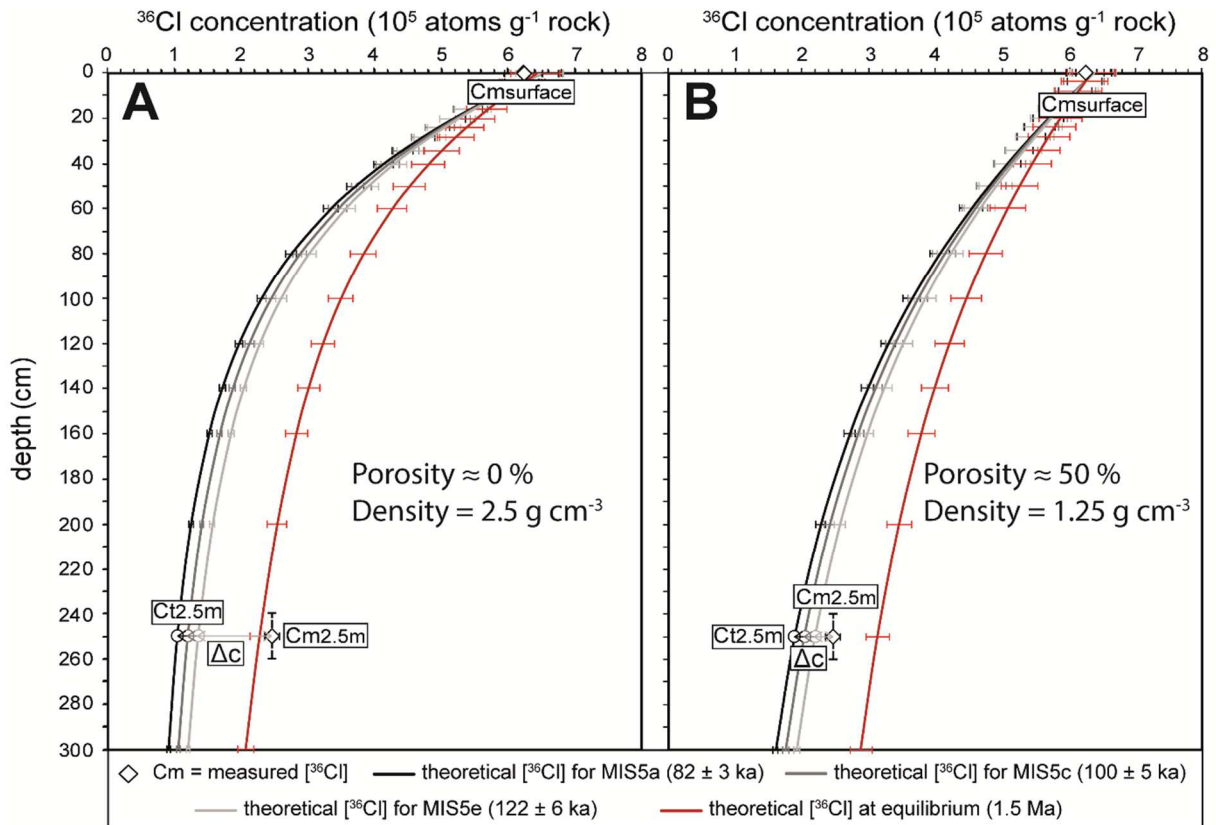
1285 **Fig. 4.** CRTs inner edges of the Cape Laundi sequence (Pleiades satellite imagery, 1  
 1286 m resolution), and the location of samples, topographic and bathymetric profiles.



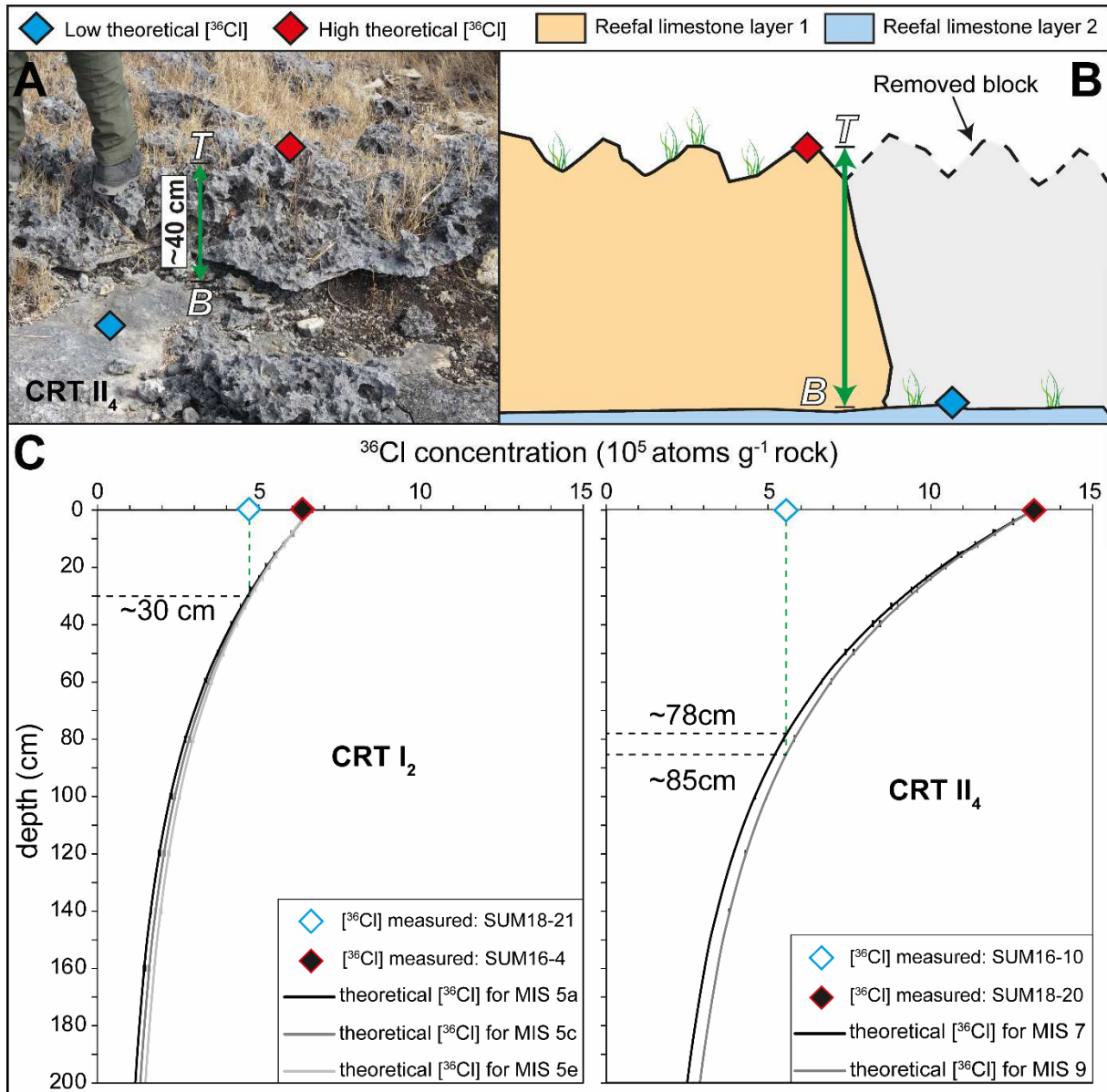
1288 **Fig. 5.** Pictures and interpretations of the Cap Laundi CRTs sequence. The elevations  
1289 result from the DGPS profile. **A)** Aerial photo of Cape Laundi showing the staircase  
1290 coastal landscape. **B)** CRT II<sub>2</sub> surface. **C)** Schematic 3D diagram of the lowest CRTs,  
1291 with locations of Figs. 5D; 5E; 5H; 5I; 5J. **D)** Smooth flat surface of CRT I<sub>1</sub>. **E)** Fossil  
1292 coral rubbles cemented within the reefal limestones outcropping on the CRT I<sub>1</sub> surface.  
1293 **F)** Cape Laundi summit. **G)** Distal edge of CRT VII. **H)** Sample SUM17-10. **I)** Sample  
1294 SUM17-13). **J)** Coral rubbles on the modern reef flat (CRT I<sub>0</sub>).



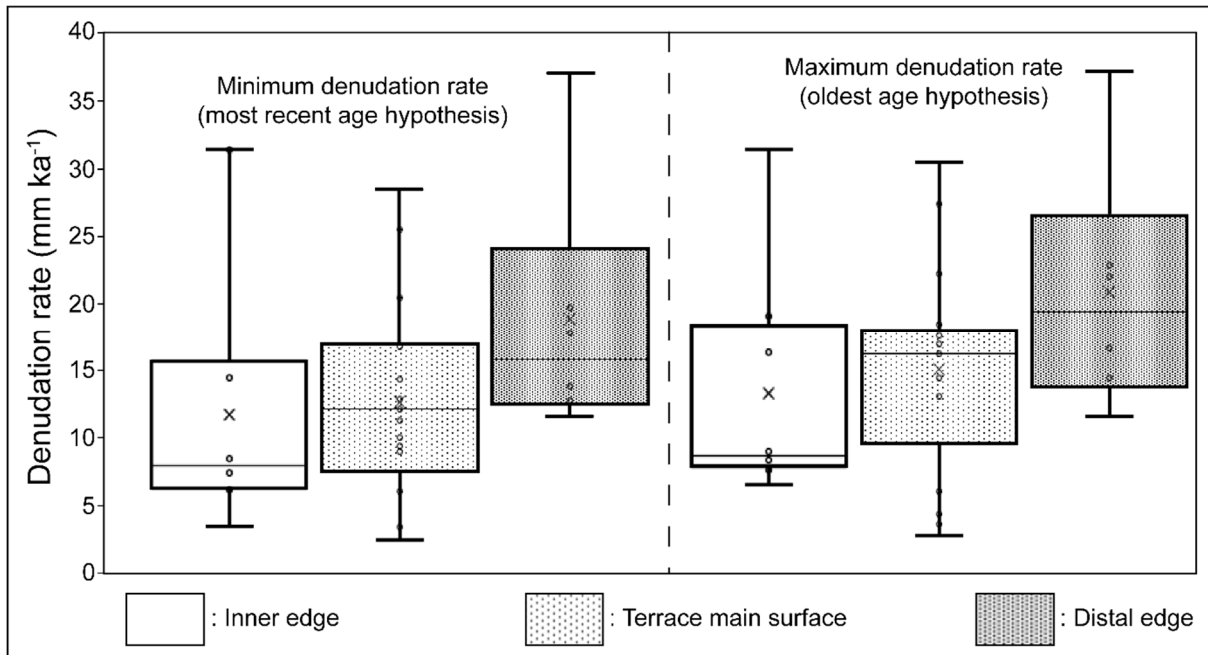
1295 **Fig. 6.** Altimetric profiles (DGPS and sonar) at Cape Laundi, showing the calculated denudation rates with various age hypotheses  
 1296 (the colors of the triangles correspond to different age hypotheses), as well as location and ages of U/Th samples (Bard et al., 1996;  
 1297 this study).



1298 **Fig. 7.** Surface ( $C_{\text{msurface}}$ ) and  $2.5 \pm 0.1$  m ( $C_{\text{m2.5m}}$ ) depth  $^{36}\text{Cl}$  concentration of the  
 1299 borehole within CRT I<sub>1</sub> for a porosity of **A**) 50 % (i.e., density =  $1.25 \text{ g cm}^{-3}$ ) and **B**) 0%  
 1300 (density =  $2.5 \text{ g cm}^{-3}$ ). Theoretical  $^{36}\text{Cl}$  concentration curves as a function of depth and  
 1301 MIS and age hypotheses.  $\Delta C$  is the difference between measured  $^{36}\text{Cl}$  ( $C_{\text{m2.5m}}$ ) and  
 1302 theoretical concentrations at  $2.5 \pm 0.1$  m depth ( $C_{\text{t2.5m}}$ ).



1303 **Fig. 8.**  $^{36}\text{Cl}$  concentration variations at the scale of a CRT. **A)** Epikarstification on the  
 1304 surface of CRT II<sub>4</sub>. **B)** Schematic cross-sectional view of Figure 7A. *T* and *B*  
 1305 correspond to the top and bottom of the reefal limestone layer 1, respectively. **C)**  
 1306 Theoretical  $^{36}\text{Cl}$  concentration curves of depth for 2 samples pairs (SUM18-21/16-4  
 1307 and SUM18-20/16-10) as a function of depth and MIS and age hypotheses, assuming  
 1308 that the ages of reefal bioconstruction and exposure duration are synchronous, as  
 1309 proposed by Pirazzoli et al. (1991; 1993).



1310 **Fig. 9.** Boxplots of denudation rates, calculated with the most recent and oldest age  
 1311 hypothesis, classified by morphological zone. The crosses, inner bars, circles, upper,  
 1312 and lower outer bars represent the average, median, data, maximum and minimum  
 1313 value for  $^{36}\text{Cl}$  concentrations, respectively.

1314

1315 **Tables**

Sample (SUM)	Sample information						Sample composition		<sup>230</sup> Th/U chemistry							
	Coral species	CRT	Morphology location	Longitude (E)	Latitude (N)	Elevation (m)	Calcite (%)	Aragonite (%)	<sup>238</sup> U (μg/g)	<sup>232</sup> Th (ng/g)	( <sup>234</sup> U/ <sup>238</sup> U)	( <sup>230</sup> Th/ <sup>238</sup> U)	age uncorrected (ka)	age corrected (ka)	MIS	( <sup>234</sup> U/ <sup>238</sup> U)initial
17-10	<i>Pseudodiploria clivosa</i>	H	Distal edge	120.221	-9.52	2.0 ± 0.5	< 1	> 99	2.37 ± 0.01	1.080 ± 0.006	1.14627 ± 0.00041	0.05584 ± 0.00020	5.460 ± 0.020	5.448 ± 0.02	1	1.14854 ± 0.00040
17-13	<i>Mussismilia leptophylla</i>	H	Distal edge	120.221	-9.52	2.0 ± 0.5	< 1	> 99	3.02 ± 0.02	1.281 ± 0.007	1.1404 ± 0.0003	0.02199 ± 0.00010	2.1359 ± 0.0083	2.1252 ± 0.0098	1	1.14126 ± 0.00030

1316 **Table 1.** Results of <sup>230</sup>Th/U dating of samples SUM17-10 and SUM17-13.

1317

1318

1319

1320

1321

1322

1323

1324

1325

1326

1327

1328

1329

Sample (SUM)	Sample location, elevation, slope and Mean Annual Precipitation (MAP)							Sample composition			AMS result
	DGPS profile	CRT name	Longitude (E)	Latitude (N)	Elevation (m)	Slope (°)	MAP (mm yr <sup>-1</sup> )	Cl (target fraction) (ppm ± 0.12)	CaO (target fraction) (wt% ± 0.25)	MgO (bulk rock) (wt%)	[ <sup>36</sup> Cl] (10 <sup>5</sup> atom g <sup>-1</sup> rock)
16-1	Profile 1	I1	120.2222	-9.5272	8.4 ± 0.5	0.0	722.8	26.23	55.24	0.39	5.95 ± 0.14
16-2	Profile 1	I2	120.2213	-9.5270	12.5 ± 0.5	2.6	722.3	15.08	54.82	0.47	5.43 ± 0.13
18-22	Profile 1	I2	120.2208	-9.5270	14.4 ± 0.5	1.5	723.3	14.17	52.06	0.57	4.82 ± 0.11
16-3	Profile 1	I2	120.2198	-9.5271	17.4 ± 0.5	3.8	727.3	12.26	56.61	0.36	6.1 ± 0.14
18-21	Profile 1	I2	120.2193	-9.5278	18.5 ± 0.5	1.5	739.9	6.29	54.34	0.32	4.69 ± 0.10
16-4	Profile 1	I2	120.2185	-9.5258	20.4 ± 0.5	1.7	723.9	14.94	55.77	0.29	6.26 ± 0.14
16-6	Profile 1	II1	120.2166	-9.5266	40.7 ± 0.5	14.9	750.7	3.07	55.80	0.34	9.7 ± 0.22
11-5	Profile 1	II1	120.2154	-9.5266	54.4 ± 0.5	4.2	760.1	18.97	53.62	0.68	6.33 ± 0.14
16-8	Profile 1	II2	120.2143	-9.5269	67.5 ± 0.5	4.5	774.6	6.49	55.51	0.47	4.45 ± 0.10
16-9	Profile 1	II3	120.2128	-9.5277	80.2 ± 0.5	4.0	797.7	8.81	55.37	0.31	4.8 ± 0.11
16-10	Profile 1	II4	120.2116	-9.5279	88.1 ± 0.5	3.1	811.6	2.89	55.14	0.15	5.53 ± 0.12
18-20	Profile 1	II4	120.2104	-9.5275	94.4 ± 0.5	3.6	816.7	1.75	52.58	0.40	13.17 ± 0.31
18-19	Profile 1	II5	120.2086	-9.5274	104.0 ± 0.5	3.3	831.3	3.67	53.59	0.28	9.54 ± 0.19
18-18	Profile 1	II6	120.2075	-9.5279	113.9 ± 0.5	3.6	847.2	2.47	52.72	0.36	7.63 ± 0.17
18-17	Profile 1	II6	120.2060	-9.5284	117.9 ± 0.5	1.5	867.0	4.32	52.75	0.34	11.47 ± 0.23
18-16	Profile 1	II7	120.2039	-9.5281	127.8 ± 0.5	3.6	881.6	5.57	47.47	0.42	13.57 ± 0.26
18-15	Profile 1	II7	120.2016	-9.5280	138.6 ± 0.5	8.2	901.0	3.16	50.46	0.30	3.80 ± 0.08
18-14	Profile 1	III	120.2004	-9.5283	163.0 ± 0.5	6.0	913.9	2.16	54.33	0.24	7.20 ± 0.16
18-37	Profile 1	IV	120.1909	-9.5272	227.1 ± 0.5	6.2	987.1	4.42	51.70		20.00 ± 0.37
18-36	Profile 1	V	120.1822	-9.5266	309.5 ± 1.5	7.3	1059.6	2.87	52.19	0.20	4.04 ± 0.09
18-35	Profile 1	V	120.1777	-9.5256	327.2 ± 1.5	8.8	1073.7	2.23	53.19	0.25	8.50 ± 0.17
18-31	Profile 1	VI	120.1738	-9.5278	380.5 ± 1.5	3.5	1101.7	2.43	53.20	0.46	15.00 ± 0.28
18-33	Profile 1	VII	120.1646	-9.5275	471.6 ± 1.5	2.7	1109.8	4.06	51.42	0.20	8.01 ± 0.17
18-24	Profile 2	I1	120.2149	-9.5072	14.7 ± 0.5	14.4	765.6	38.37	52.12	0.51	7.26 ± 0.16
18-25	Profile 2	I2	120.2144	-9.5074	25.8 ± 0.5	3.1	767.4	7.37	52.29	0.29	3.68 ± 0.08
18-26	Profile 2	II0	120.2132	-9.5075	35.2 ± 0.5	7.0	774.4	49.08	51.88	0.63	8.31 ± 0.21
18-28	Profile 2	II1	120.2123	-9.5075	43.3 ± 0.5	10.6	779.6	3.96	53.32	0.50	5.11 ± 0.11
18-27	Profile 2	II1	120.2118	-9.5076	56.1 ± 0.5	12.1	782.4	9.24	51.62	0.29	5.11 ± 0.11
Cmsurface	Borehole	I1	120.2237	-9.5336	2.8 ± 0.5	0.0	790.6	12.26	56.61	0.36	6.23 ± 0.14
Cm2.5m	Borehole	I1	120.2237	-9.5336	-2.5 ± 0.1			18.15	52.49	0.75	2.46 ± 0.06
18-46	Off profile	I1	120.2207	-9.5179	2.0 ± 0.5	0.0	638.9	245.15	47.14	2.67	0.38 ± 0.04
18-47	Off profile	I0	120.2207	-9.5179	0.0	0.0	638.9	178.84	49.93	1.43	0.30 ± 0.03
11-6	Off profile	II6	120.2009	-9.5217	149.3 ± 0.5	2.1	830.8	3.38	55.33	0.38	10.82 ± 0.23
14-2	Off profile	IV	120.1139	-9.5274	210.8 ± 0.5	3.5	1094.4	2.22	55.33	0.26	7.07 ± 0.15
14-2	Off profile	V	120.1141	-9.5407	293.9 ± 1.5	3.4	1142.8	1.97	55.69	0.14	8.27 ± 0.18

1330 **Table 2.** Bedrock sample information, location, elevation, chemical composition, and AMS <sup>36</sup>Cl results. Mean annual precipitation  
1331 (MAP) values are TRMM data (e.g., Kummerow et al., 2000).

Sample (SUM)	Morphology location	AMS result [ <sup>36</sup> C] (10 <sup>9</sup> atom g <sup>-1</sup> )	Hypothesis 1			Hypothesis 2			Hypothesis 3			Mean denudation rate (mm ka <sup>-1</sup> )	Integration time (ka)
			MIS	Exposure duration (ka)	Denudation rate (mm ka <sup>-1</sup> )	MIS	Exposure duration (ka)	Denudation rate (mm ka <sup>-1</sup> )	MIS	Exposure duration (ka)	Denudation rate (mm ka <sup>-1</sup> )		
16-1	Terrace main surface	5.95 ± 0.14	5a	82 ± 3	11.3 ± 0.1	5c	100 ± 5	13.7 ± 0.1	5e	122 ± 6	16.2 ± 0.1	13.7 ± 2.5	44.7 ± 8.0
16-2	Terrace main surface	5.43 ± 0.13	5a	82 ± 3	12.1 ± 0.1	5c	100 ± 5	14.4 ± 0.1	5e	122 ± 6	18.4 ± 0.1	15.0 ± 3.2	41.2 ± 8.5
18-22	Terrace main surface	4.82 ± 0.11	5a	82 ± 3	12.8 ± 0.4	5c	100 ± 5	175.1 ± 0.4	5e	122 ± 6	16.9 ± 0.4	14.9 ± 2.1	40.7 ± 5.7
16-3	Terrace main surface	6.1 ± 0.14	5a	82 ± 3	10.0 ± 0.1	5c	100 ± 5	12.5 ± 0.1	5e	122 ± 6	14.4 ± 0.1	12.3 ± 2.2	49.9 ± 9.3
18-21	Terrace main surface	4.69 ± 0.10	5a	82 ± 3	13.0 ± 0.4	5c	100 ± 5	15.2 ± 0.4	5e	122 ± 6	17.1 ± 0.4	15.1 ± 2.1	40.3 ± 5.7
16-4	Terrace main surface	6.26 ± 0.14	5a	82 ± 3	8.9 ± 0.1	5c	100 ± 5	11.3 ± 0.1	5e	122 ± 6	13.1 ± 0.1	11.1 ± 2.1	55.5 ± 11.3
16-6	Inner edge	9.7 ± 0.22	5e	122 ± 6	3.4 ± 0.0(2)	7e	239.5 ± 8.5	7.6 ± 0.0(2)				5.5 ± 2.9	127.9 ± 68.6
11-5	Distal edge	6.33 ± 0.14	5e	122 ± 6	12.8 ± 0.1	7e	239.5 ± 8.5	16.7 ± 0.1				14.7 ± 2.8	41.6 ± 7.8
16-8	Terrace main surface	4.45 ± 0.10	7e	239.5 ± 8.5	28.4 ± 0.2	9e	325 ± 18.5	30.4 ± 0.2				29.4 ± 1.4	20.4 ± 1.0
16-9	Terrace main surface	4.8 ± 0.11	7e	239.5 ± 8.5	25.4 ± 0.2	9e	325 ± 18.5	27.3 ± 0.2				26.4 ± 1.3	22.8 ± 1.1
16-10	Terrace main surface	5.53 ± 0.12	7e	239.5 ± 8.5	20.4 ± 0.1	9e	325 ± 18.5	22.1 ± 0.1				21.3 ± 1.2	28.3 ± 1.6
18-20	Terrace main surface	13.17 ± 0.31	7e	239.5 ± 8.5	3.4 ± 0.1	9e	325 ± 18.5	4.4 ± 0.1				3.9 ± 0.7	156.0 ± 26.8
18-19	Inner edge	9.54 ± 0.19	7e	239.5 ± 8.5	7.4 ± 0.2	9e	325 ± 18.5	8.3 ± 0.2				7.8 ± 0.7	76.8 ± 6.4
18-18	Distal edge	7.63 ± 0.17	9e	325 ± 18.5	11.6 ± 0.3							11.6 ± 0.3	51.7 ± 0.1
18-17	Terrace main surface	11.47 ± 0.23	9e	325 ± 18.5	6.0 ± 0.1							6.0 ± 0.1	99.5 ± 0.1
18-16	Terrace main surface	13.57 ± 0.26	9e	325 ± 18.5	3.6 ± 0.1							3.6 ± 0.1	164.8 ± 0.1
18-15	Inner edge	3.80 ± 0.08	9e	325 ± 18.5	31.3 ± 0.8							31.3 ± 0.8	19.2 ± 0.1
18-14	Distal edge	7.20 ± 0.16	9e	325 ± 18.5	13.8 ± 0.4	11c	390 ± 30	14.4 ± 0.4				14.1 ± 0.4	42.5 ± 1.4
18-37	Terrace main surface	20.00 ± 0.37	11c	390 ± 30	2.3 ± 0.1	13a	495 ± 15	2.8 ± 0.1				2.5 ± 0.3	237.3 ± 27.0
18-36	Distal edge	4.04 ± 0.09	15e	610 ± 10	37.0 ± 0.9	17c	695 ± 15	37.1 ± 0.9				37.1 ± 0.1	16.2 ± 0.3
18-35	Terrace main surface	8.50 ± 0.17	15e	610 ± 10	14.3 ± 0.3	17c	685 ± 15	14.4 ± 0.3				14.4 ± 0.1	41.8 ± 0.3
18-31	Inner edge	15.00 ± 0.28	19	780 ± 10	6.4 ± 0.1	21	850 ± 15	6.5 ± 0.1	23	910 ± 10	6.6 ± 0.1	6.5 ± 0.1	92.4 ± 0.8
18-33	Terrace main surface	8.01 ± 0.17	27	980 ± 5	17.1 ± 0.4	29	1020 ± 10	17.2 ± 0.4				17.2 ± 0.0(1)	35.0 ± 0.1
18-24	Inner edge	7.26 ± 0.16	5a	82 ± 3	6.1 ± 0.2	5c	100 ± 5	8.9 ± 0.2	5e	122 ± 6	10.8 ± 0.2	8.6 ± 2.4	73.8 ± 22.1
18-25	Distal edge	3.68 ± 0.08	5a	82 ± 3	19.7 ± 0.5	5c	100 ± 5	22.0 ± 0.5	5e	122 ± 6	24.0 ± 0.2	21.9 ± 2.2	27.6 ± 2.8
18-26	Terrace main surface	8.31 ± 0.21	5e	122 ± 6	9.4 ± 0.2	7e	239.5 ± 8.5	13.0 ± 0.2				11.2 ± 2.6	55.1 ± 12.8
18-28	Inner edge	5.11 ± 0.11	5e	122 ± 6	14.4 ± 0.4	7e	239.5 ± 8.5	19.0 ± 0.4				16.7 ± 3.3	36.6 ± 7.1
18-27	Distal edge	5.11 ± 0.11	5e	122 ± 6	17.8 ± 0.5	7e	239.5 ± 8.5	22.8 ± 0.5				20.3 ± 3.5	30.0 ± 5.3
18-46	Distal edge	0.38 ± 0.04	Holocene	2.13 ± 0.01	279.0 ± 0.4	Holocene	5.45 ± 0.02	581.0 ± 0.4				430 ± 214	1.6 ± 2.8
11-6	Inner edge	10.82 ± 0.23	9e	325 ± 18.5	8.4 ± 0.2							8.4 ± 0.2	71.4 ± 0.1
14-1	Terrace main surface	7.07 ± 0.15	11c	390 ± 30	16.8 ± 0.4	13a	495 ± 15	17.5 ± 0.4				17.1 ± 0.5	35.0 ± 1.1
14-2	Inner edge	8.27 ± 0.18	15e	610 ± 10	16.1 ± 0.4	17c	685 ± 15	16.3 ± 0.4				16.2 ± 0.1	37.0 ± 0.3

1332

1333 **Table 3.** Morphology location and calculated denudation rates from the  $^{36}\text{Cl}$  concentrations and the different MIS and age hypotheses,  
1334 assuming that the ages of reefal bioconstruction and exposure duration are synchronous, for each CRT of the sequence as proposed  
1335 by Pirazzoli et al. (1991; 1993). The MIS ages and their uncertainties are derived from Cutler et al. (2003) and Murray-Wallace and  
1336 Woodroffe (2014). Denudation rate uncertainties are calculated by standard error propagation, including uncertainties from production  
1337 rates, ages, and AMS measurements. Mean denudation rate uncertainties are calculated using the standard deviation.

Porosity %	Density (g cm <sup>-3</sup> )	Ed		Denudation rate (mm ka <sup>-1</sup> )	Ct2.5m (10 <sup>5</sup> atoms g rock <sup>-1</sup> )	$\Delta c$ (10 <sup>5</sup> atoms g rock <sup>-1</sup> )	Ed $\Delta c$ ka
		MIS	ka				
50	1.25	5a	82 ± 3	20.0 ± 0.2	1.88 ± 0.03	0.58 ± 0.15	5.4 ± 1.3
		5c	100 ± 5	24.9 ± 0.2	2.02 ± 0.03	0.44 ± 0.15	4.0 ± 1.2
		5e	122 ± 6	28.6 ± 0.3	2.18 ± 0.03	0.28 ± 0.15	2.6 ± 1.2
0	2.5	5a	82 ± 3	9.5 ± 0.2	1.05 ± 0.03	1.41 ± 0.15	13.8 ± 1.3
		5c	100 ± 5	11.9 ± 0.2	1.19 ± 0.03	1.27 ± 0.15	12.5 ± 1.2
		5e	122 ± 6	13.8 ± 0.3	1.34 ± 0.03	1.15 ± 0.15	11.0 ± 1.2

1338 **Table 4.** Borehole <sup>36</sup>Cl theoretical concentrations and theoretical exposure duration within CRT I<sub>1</sub>. Ed, MIS, Ct2.5m,  $\Delta c$ , Ed $\Delta c$ ,  
1339 correspond to the exposure duration for surface sample (Cmsurface), Marine Isotope Stage, <sup>36</sup>Cl theoretical concentration at 2.5 ±  
1340 0.1 m depth (Ct2.5m) calculated from the <sup>36</sup>Cl measured concentration of the surface sample, the difference between <sup>36</sup>Cl measured  
1341 (Cm2.5m) and theoretical concentrations at 2.5 ± 0.1 m depth (Ct2.5m), the theoretical exposure duration calculated from  $\Delta c$ ,  
1342 respectively. The ages and their uncertainties are derived from Cutler et al. (2003) and Murray-Wallace and Woodroffe (2014).